

SOURCE
DATATRANSPARENT
PROCESSOPEN
ACCESS

RBPJ/CBF1 interacts with L3MBTL3/MBT1 to promote repression of Notch signaling via histone demethylase KDM1A/LSD1

Tao Xu^{1,§}, Sung-Soo Park^{1,§}, Benedetto Daniele Giaimo^{2,§}, Daniel Hall³, Francesca Ferrante², Diana M Ho⁴, Kazuya Hori^{4,†}, Lucas Anhezini^{5,‡}, Iris Ertl^{6,¶}, Marek Bartkuhn⁷, Honglai Zhang¹, Eléna Milon¹, Kimberly Ha¹, Kevin P Conlon¹, Rork Kuick⁸, Brandon Govindarajoo⁹, Yang Zhang⁹, Yuqing Sun¹, Yali Dou¹, Venkatesha Basrur¹, Kojo SJ Elenitoba-Johnson¹, Alexey I Nesvizhskii^{1,9}, Julian Ceron⁶, Cheng-Yu Lee⁵, Tilman Borggrefe², Rhett A Kovall³ & Jean-François Rual^{1,*} 

Abstract

Notch signaling is an evolutionarily conserved signal transduction pathway that is essential for metazoan development. Upon ligand binding, the Notch intracellular domain (NOTCH ICD) translocates into the nucleus and forms a complex with the transcription factor RBPJ (also known as CBF1 or CSL) to activate expression of Notch target genes. In the absence of a Notch signal, RBPJ acts as a transcriptional repressor. Using a proteomic approach, we identified L3MBTL3 (also known as MBT1) as a novel RBPJ interactor. L3MBTL3 competes with NOTCH ICD for binding to RBPJ. In the absence of NOTCH ICD, RBPJ recruits L3MBTL3 and the histone demethylase KDM1A (also known as LSD1) to the enhancers of Notch target genes, leading to H3K4me2 demethylation and to transcriptional repression. Importantly, *in vivo* analyses of the homologs of RBPJ and L3MBTL3 in *Drosophila melanogaster* and *Caenorhabditis elegans* demonstrate that the functional link between RBPJ and L3MBTL3 is evolutionarily conserved, thus identifying L3MBTL3 as a universal modulator of Notch signaling in metazoans.

Keywords KDM1A; L3MBTL3; Notch signaling; RBPJ

Subject Categories Signal Transduction; Transcription

DOI 10.15252/embj.201796525 | Received 13 January 2017 | Revised 31 August 2017 | Accepted 12 September 2017 | Published online 13 October 2017

The EMBO Journal (2017) 36: 3232–3249

Introduction

The Notch signal transduction pathway is a conserved signaling mechanism that is fundamental for morphogenesis in multicellular organisms (Bray, 2006; Kopan & Ilagan, 2009; Hori *et al.*, 2013). The biological action of Notch is highly pleiotropic, and impaired Notch signaling leads to a broad spectrum of developmental disorders (Louvi & Artavanis-Tsakonas, 2012) and many types of cancer (Aster *et al.*, 2017). The developmental outcome of Notch signaling is strictly dependent on the cell context and can influence cell fate in a remarkable number of different ways, for example, differentiation, proliferation, and apoptosis (Bray, 2006; Kopan & Ilagan, 2009; Hori *et al.*, 2013). Thus, various context-specific mechanisms, many of which likely remain to be uncovered, allow the Notch building block to be “re-used” in different flavors at various junctures within the developmental framework. Identifying these context-specific modulators of Notch signaling is not only essential to understanding the plasticity of Notch as a regulator of cell fate during morphogenesis, but it could also provide novel clues to manipulating Notch for therapeutic benefit in human diseases.

At the molecular level, canonical Notch signaling involves the binding of a membrane-bound DSL (Delta, Serrate, Lag-2)-family ligand presented on the cell surface of one cell to the Notch transmembrane receptor located on a neighboring cell (Bray, 2006; Kopan & Ilagan, 2009; Hori *et al.*, 2013). Upon ligand

1 Department of Pathology, University of Michigan Medical School, Ann Arbor, MI, USA

2 Institute of Biochemistry, University of Giessen, Giessen, Germany

3 Department of Molecular Genetics, Biochemistry and Microbiology, University of Cincinnati College of Medicine, Cincinnati, OH, USA

4 Department of Cell Biology, Harvard Medical School, Boston, MA, USA

5 Life Sciences Institute, University of Michigan, Ann Arbor, MI, USA

6 Cancer and Human Molecular Genetics, Bellvitge Biomedical Research Institute, L'Hospitalet de Llobregat, Barcelona, Spain

7 Institute for Genetics, University of Giessen, Giessen, Germany

8 Center for Cancer Biostatistics, School of Public Health, University of Michigan, Ann Arbor, MI, USA

9 Department of Computational Medicine & Bioinformatics, University of Michigan, Ann Arbor, MI, USA

*Corresponding author. Tel: +1 734 764 6975; E-mail: jrual@umich.edu

§These authors contributed equally to this work

†Present address: Department of Pharmacology, University of Fukui, Fukui, Japan

‡Present address: Instituto de Ciências Biológicas e Naturais, Universidade Federal do Triângulo Mineiro, Uberaba, MG, Brazil

¶Present address: Department of Urology, Medical University of Vienna, Vienna, Austria

binding, the NOTCH receptor is processed by proteolytic cleavages, leading to the release of its intracellular domain (NOTCH ICD) into the cytoplasm. NOTCH ICD traffics to the nucleus and complexes with the DNA-binding transcription factor CSL to regulate target genes. The *CSL* gene, which is the main focus of this study, is also known as *CBF1/RBPJ* in vertebrates, *Suppressor of Hairless [Su(H)]* in *Drosophila melanogaster*, and *lag-1* in *Caenorhabditis elegans*. As previously observed for Su(H) in *Drosophila*, mammalian RBPJ has a dual role in regulating Notch signaling (Bray, 2006; Kopan & Ilagan, 2009; Tanigaki & Honjo, 2010). Upon Notch activation, NOTCH ICD, RBPJ, and additional co-activators form the Notch transcriptional activation complex (NTC) that supports the expression of target genes (Wang *et al*, 2015). In the absence of NOTCH ICD, RBPJ interacts with multiple transcriptional co-repressors, for example, KYOT2 or MINT and inhibits transcription of Notch target genes (Borggreffe & Oswald, 2014). As such, the role of RBPJ is multifaceted and context dependent (Bray, 2006; Kopan & Ilagan, 2009; Tanigaki & Honjo, 2010). In some contexts, for example, marginal zone B-cell development (Zhang *et al*, 2012) or maintenance of muscle progenitor cells (Vasyutina *et al*, 2007), loss of *RBPJ* results in the inhibition of Notch target genes and blocks the regulation of Notch-driven physiological states. In other contexts, for example, maintenance of adult neural stem cell population (Fujimoto *et al*, 2009) or breast tumorigenesis (Kulic *et al*, 2015), loss of *RBPJ* contributes to the “de-repression” of Notch target genes and results in the promotion of biological processes that are otherwise suppressed in the absence of Notch signaling. Identifying the molecular partners of RBPJ will help to better understand the complex and context-dependent role of RBPJ in the regulation of Notch signaling in both normal and disease contexts.

We generated a map of the Notch molecular network by using two complementary proteomic approaches: affinity purification coupled to mass spectrometry analysis (AP-MS) and the yeast two-hybrid assay (Y2H). Here, we focus on the characterization of one of our RBPJ proteomic hits: L3MBTL3 (also known as MBT1). L3MBTL3 [lethal (3) malignant brain tumor-like 3] is a poorly characterized member of the MBT (malignant brain tumor) family of methyl-lysine readers that act as chromatin-interacting transcriptional repressors (Bonasio *et al*, 2010; Nady *et al*, 2012). In the case of L3MBTL1, a paralog of L3MBTL3, its MBT domains promote binding to methyl-lysines within histone proteins (Min *et al*, 2007; Nady *et al*, 2012), leading to chromatin compaction and repression (Trojer *et al*, 2007), or within non-histone proteins, for example, p53 (West *et al*, 2010). L3MBTL3 contains three MBT domains, whose functions remain to be characterized. In mice, loss of *L3MBTL3* leads to impaired maturation of myeloid progenitors causing the *L3MBTL3*^{-/-} mice to die of anemia at a late embryonic stage (E18) (Arai & Miyazaki, 2005).

In this report, we show that L3MBTL3 physically and functionally interacts with RBPJ. L3MBTL3 co-localizes with RBPJ on chromatin and contributes to the recruitment of the histone demethylase KDM1A [lysine (K)-specific demethylase 1A, also known as LSD1] at Notch target genes, thus resulting in their transcriptional repression. Finally, the genetic analyses of the homologs of *RBPJ* and *L3MBTL3* in *Drosophila* and *C. elegans* suggest that the functional link between these two genes is evolutionarily conserved across metazoans.

Results

The RBPJ/L3MBTL3 interaction

To identify novel RBPJ interactors, we performed a proteomic screen and obtained multiple independent lines of evidence supporting a molecular interaction between RBPJ and L3MBTL3. First, we identified the RBPJ/L3MBTL3 interaction in a Y2H proteomic screen (Fig 1A). Second, we performed duplicate AP-MS experiments for HA-tagged RBPJ in U87-MG cells. The MS analysis of the purified protein extracts unveiled: (i) the successful purification of HA-RBPJ with 169 and 494 MS spectra matching the RBPJ protein sequence in the AP-MS experiments #1 and #2, respectively; (ii) the co-purification of previously known RBPJ interactors, for example, NOTCH2, MINT, and KYOT2 (Taniguchi *et al*, 1998; Oswald *et al*, 2002); and (iii) the co-purification of endogenous L3MBTL3, with six and 17 MS spectra matching L3MBTL3 protein sequence in AP-MS experiments #1 and #2, respectively (Table EV1). In a reciprocal AP-MS experiment using HA-tagged L3MBTL3 as a bait, 124 MS spectra matching L3MBTL3 protein sequence were observed, validating the successful purification of HA-L3MBTL3. In addition, three MS spectra matching RBPJ protein sequence were observed in this L3MBTL3 AP-MS experiment (Table EV1), further supporting the Y2H data.

Next, we performed immuno-precipitations (IPs) of HA-tagged RBPJ or HA-tagged L3MBTL3 in U87-MG cells followed by Western blot analyses using RBPJ or L3MBTL3 antibody. We observed that endogenous L3MBTL3 co-purifies with HA-RBPJ and that endogenous RBPJ co-purifies with HA-L3MBTL3 (Fig 1B and C). In support of our data, the RBPJ/L3MBTL3 interaction was also recently uncovered in a large-scale proteomic analysis, using a tandem AP-MS approach in HEK293T cells (Li *et al*, 2015b). We further validated the RBPJ/L3MBTL3 interaction by performing reciprocal IPs in HEK293T cells in which HA-tagged RBPJ and MYC-tagged or SBP-FLAG-tagged L3MBTL3 were co-expressed (Appendix Fig S1A). Finally, we performed GST pulldowns with bacteria-purified RBPJ and *in vitro*-transcribed/translated L3MBTL3 proteins (Appendix Fig S1B–D). The results of these GST pulldown experiments validate the RBPJ/L3MBTL3 interaction and demonstrate a direct interaction, as suggested by the Y2H experiment (Appendix Fig S1B and C). In addition, dividing the L3MBTL3 protein in two partially overlapping fragments, we observed that the RBPJ/L3MBTL3 interaction is mediated by a domain located in the N-terminal end of L3MBTL3 (Appendix Fig S1B and D). Altogether, these data demonstrate the direct RBPJ/L3MBTL3 interaction.

Mapping the RBPJ/L3MBTL3 interaction

As a first step toward the characterization of the molecular interplay between RBPJ and L3MBTL3, a series of L3MBTL3 deletion mutants were employed to identify its RBPJ-interacting domain(s) (Fig 2A). In IP experiments, we observed that the MBT, ZnF, and SAM domains are not required for the RBPJ/L3MBTL3 interaction (Fig 2B). In contrast, we observed that the deletion of the L3MBTL3-(1-64) domain strongly impairs the interaction with RBPJ, supporting an important role for this domain in the mediation of the RBPJ/L3MBTL3 interaction (Fig 2B).

Similarly, we tested various mutants of RBPJ for their ability to interact with L3MBTL3 (Fig 2C). We observed that the N-terminal

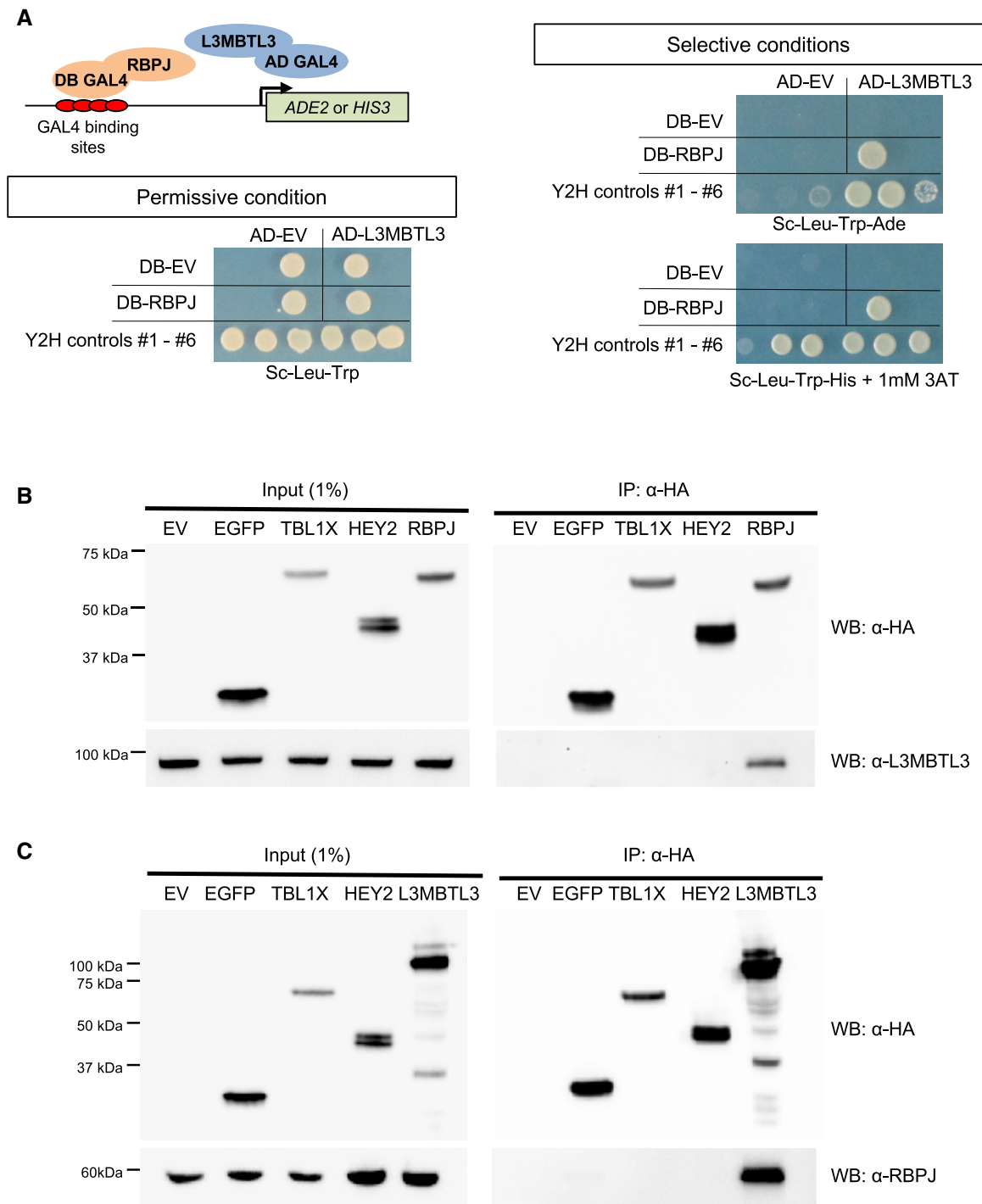


Figure 1. RBPJ interacts with L3MBTL3.

A Detection of the RBPJ/L3MBTL3 interaction using the yeast two-hybrid (Y2H) assay. In this Y2H experiment, RBPJ is fused to the GAL4 DNA-binding (DB) domain and L3MBTL3 is fused to the GAL4 activation domain (AD). The DB-RBPJ and AD-L3MBTL3 fusion proteins interact with each other, leading to the activation of the *ADE2* and *HIS3* reporter genes and allowing yeast cells to grow on selective media lacking adenine or histidine. The six Y2H controls were previously described (Dreze *et al*, 2010). The experiment was independently replicated thrice.

B Endogenous L3MBTL3 co-purifies specifically with HA-RBPJ but not with HA-EGFP, HA-TBL1X, or HA-HEY2. Immunoprecipitation (IP) of HA-tagged RBPJ, EGFP, TBL1X, or HEY2 in U87-MG cells followed by Western blot analyses using HA or L3MBTL3 antibody. The experiment was independently replicated twice.

C Endogenous RBPJ co-purifies specifically with HA-L3MBTL3 but not with HA-EGFP, HA-TBL1X, or HA-HEY2. IPs of HA-tagged L3MBTL3, EGFP, TBL1X, or HEY2 in U87-MG cells followed by Western blot analyses using HA or RBPJ antibody. The experiment was independently replicated twice.

Data information: EV, empty vector control; WB, Western blot; IP, immunoprecipitation.

Source data are available online for this figure.

domain (NTD) and C-terminal domain (CTD) of RBPJ are not required for the L3MBTL3 interaction (Fig 2D). In contrast, we observed that the absence of the β -trefoil domain (BTD) strongly impairs the RBPJ/L3MBTL3 interaction (Fig 2D). As we narrowed down our analysis to single missense mutants, we identified three L3MBTL3 interaction-defective mutants of RBPJ: RBPJ^{F261R}, RBPJ^{V263R}, and RBPJ^{A284R} (Fig 2E). Interestingly, the F261, V263, and A284 residues are located in the BTD domain and are also required for the RBPJ/NOTCH ICD interaction (Yuan *et al*, 2012). These observations suggest a molecular model in which NOTCH ICD and L3MBTL3 bind to the same interaction interface in the BTD domain and may therefore compete for binding to RBPJ.

Thermodynamic analysis of the RBPJ/L3MBTL3 interaction

To estimate the thermodynamic binding parameters that underlie the RBPJ/L3MBTL3 interaction, we used isothermal titration calorimetry (ITC) with highly purified preparations of recombinant RBPJ and L3MBTL3 proteins (Fig 3A and Table 1). The L3MBTL3-(31-70) domain mediates a 1:1 interaction with RBPJ that is characterized by a moderate binding affinity ($K_d = 0.45 \mu\text{M}$). These data suggest that, under cell-free settings, the N-terminal region of L3MBTL3 supports the interaction with RBPJ. The affinity between RBPJ and L3MBTL3 is stronger than the one previously measured, under identical conditions, between RBPJ and the viral co-activator EBNA2 ($K_d = 4.6 \mu\text{M}$) (Johnson *et al*, 2010). However, the binding affinity of the RBPJ/L3MBTL3 interaction is weaker than the ones observed for the RBPJ interactors NOTCH ICD-RAM ($K_d = 22 \text{ nM}$) (Friedmann *et al*, 2008), KyoT2 ($K_d = 12 \text{ nM}$) (Collins *et al*, 2014) and MINT ($K_d = 11 \text{ nM}$) (VanderWielen *et al*, 2011).

If, as suggested by the results of our mapping experiments (Fig 2D and E), NOTCH ICD competes with L3MBTL3 for binding to RBPJ, our K_d measurements suggest that NOTCH ICD has a significantly higher affinity (Fig 3A and Table 1) and would therefore likely outcompete L3MBTL3 for binding to RBPJ. To verify this hypothesis, we performed a competition IP assay in which the RBPJ/L3MBTL3 interaction is tested in the presence of an increasing amount of NOTCH1 ICD. As shown in Fig 3B, the RBPJ/L3MBTL3 interaction is strongly impaired in the presence of NOTCH1 ICD in a dose-dependent manner. We note that an approximately equal amount of NOTCH1 ICD displaces most L3MBTL3 molecules from RBPJ complexes (Fig 3B) but that the reciprocal is not observed, that is, L3MBTL3 does not displace NOTCH1 ICD from RBPJ (Fig 3C),

corroborating the results of our ITC experiment, that is, L3MBTL3 binds to RBPJ with a moderate affinity ($K_d = 0.45 \mu\text{M}$), which is about 20-fold weaker than the one previously observed for the RBPJ/NOTCH ICD interaction ($K_d = 22 \text{ nM}$) (Friedmann *et al*, 2008).

L3MBTL3 acts as a negative regulator of Notch target genes

RBPJ has a dual role in the regulation of Notch signaling, that is, depending on the cell context, depletion of RBPJ can result either in the inhibition or in the activation (“de-repression”) of Notch target genes. In U87-MG cells, where Notch signaling tone is low (Appendix Fig S2), we observed that the depletion of RBPJ results in the upregulation of the Notch target genes *HES1*, *HES4*, *HEY1*, and *HEY2* (Fig 4A), suggesting that RBPJ protein complexes are actively involved in the repression of Notch target genes in this context. As a RBPJ co-factor, L3MBTL3 may also contribute to the RBPJ-mediated repression of Notch target genes in U87-MG cells. To test this hypothesis, we evaluated the effects of depletion of L3MBTL3 on gene expression. As shown in Fig 4B, the CRISPR/Cas9-mediated loss of *L3MBTL3* leads to upregulation of *HES1*, *HES4*, *HEY1*, and *HEY2*, suggesting that L3MBTL3 actively contributes to the repression of Notch target genes in U87-MG cells.

We hypothesized that L3MBTL3 forms a chromatin-bound complex with RBPJ at the Notch-responsive elements of Notch target genes to repress their expression. To test this hypothesis, we performed chromatin immuno-precipitation (ChIP) experiments in U87-MG cells to determine whether L3MBTL3 localizes at the RBPJ-bound Notch-responsive elements of *HES1*, *HES4*, *HEY1*, and *HEY2* (either proximal or distal to the promoter; represented in Appendix Fig S3A). Our results indicate that L3MBTL3 co-localizes with RBPJ at the Notch-responsive elements of these Notch target genes (Fig 4C and Appendix Fig S3B and C). To investigate the RBPJ dependence of L3MBTL3 binding at these sites, we performed ChIP in U87-MG cells in the presence (sh-Scramble control cells, or “sh-Scr”) or absence (sh-*RBPJ* RNAi-mediated knockdown) of RBPJ. We observed that the depletion of RBPJ results in a strong reduction of L3MBTL3 occupancy at the proximal Notch-responsive elements of Notch target genes (Fig 4D). We note that the reciprocal was not observed, as the knockout (KO) of *L3MBTL3* has no effect on the binding of RBPJ (Appendix Fig S3D).

To further investigate the extent to which L3MBTL3’s ability to regulate Notch signaling directly depends on the presence of RBPJ, we analyzed the expression of Notch target genes in U87-MG cells in

Figure 2. Mapping of the RBPJ/L3MBTL3 interaction.

- Schematic representation of the L3MBTL3 protein and the deletion mutants used in panel (B). The L3MBTL3 protein (XP_006715641.1) consists of a C2C2 zinc finger (ZnF #1; CDD: 128717), three MBT domains (CDD: 214723), a C2H2 zinc finger (ZnF #2; CDD: 201844), and a sterile α motif domain (SAM; CDD: 197735).
- L3MBTL3- Δ (1-64) does not interact with RBPJ. IP of HA-FLAG-tagged RBPJ in the presence of FLAG-tagged L3MBTL3 (WT or deletion mutants) in HEK293T cells followed by Western blotting using FLAG antibody. The experiment was independently replicated twice.
- Schematic representation of the RBPJ protein and the deletion mutants used in panels (D and E). The RBPJ protein (XP_005248218.1) consists of the N-terminal domain (NTD), the β -trefoil domain (BTD), and the C-terminal domain (CTD).
- Deletion of the BTD domain impairs the RBPJ/L3MBTL3 interaction. IP of HA-tagged L3MBTL3 in the presence of FLAG-tagged RBPJ (WT and deletion mutants) in HEK293T cells followed by Western blotting using HA or FLAG antibody. The experiment was independently replicated twice.
- RBPJ^{F261R} point mutant does not interact with L3MBTL3. IP of HA-tagged L3MBTL3 in the presence of FLAG-tagged RBPJ (WT and point mutants) in HEK293T cells followed by Western blotting using HA or FLAG antibody. RBPJ^{V263R} and RBPJ^{A284R} also show a reduced ability to interact with L3MBTL3. The experiment was independently replicated twice.

Data information: WB, Western blot; IP, immuno-precipitation.

Source data are available online for this figure.

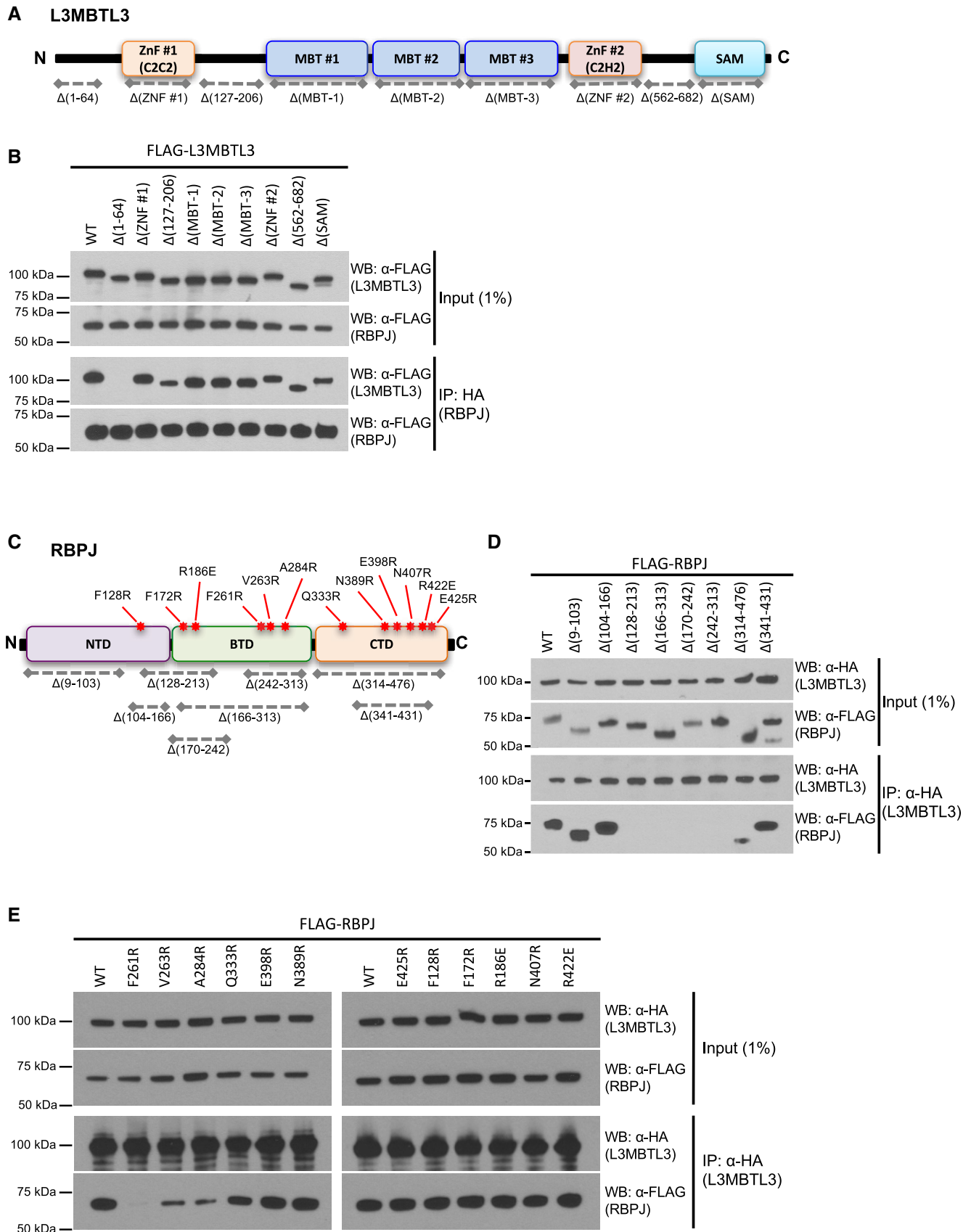


Figure 2.

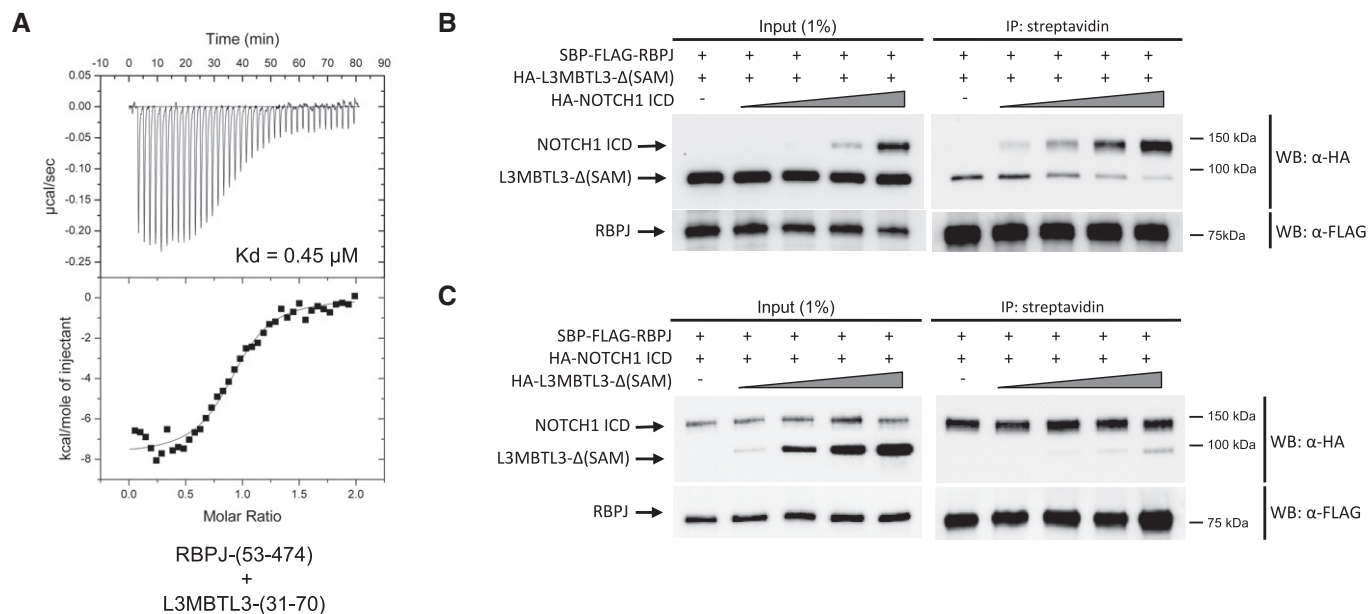


Figure 3. NOTCH1 ICD and L3MBTL3 compete for binding to RBPJ.

A Thermodynamic characterization of the RBPJ/L3MBTL3 interaction. Representative thermograms (raw heat signal and nonlinear least squares fit to the integrated data) for L3MBTL3-(31-70) binding to RBPJ-(53-474).

B, C NOTCH1 ICD outcompetes L3MBTL3 for binding to RBPJ in a dose-dependent manner. IPs were performed in CRISPR/Cas9-mediated *L3MBTL3* knockout (KO) HEK293T cells. (B) SBP-FLAG-RBPJ and HA-L3MBTL3- Δ (SAM) in the presence of an increasing amount of HA-NOTCH1 ICD. (C) SBP-FLAG-RBPJ and HA-NOTCH1 ICD in the presence of an increasing amount of HA-L3MBTL3- Δ (SAM). The L3MBTL3- Δ (SAM) mutant construct was used instead of the L3MBTL3 WT construct in order to allow the analysis of both NOTCH1 ICD and L3MBTL3 proteins in the same Western blot. CRISPR/Cas9 sg-*L3MBTL3*-resistant plasmids were used to express HA-L3MBTL3- Δ (SAM). The experiment was independently replicated thrice. WB, Western blot; IP, immuno-precipitation.

Source data are available online for this figure.

the presence (sh-Scr) or absence of RBPJ (sh-*RBPJ*), upon overexpression of L3MBTL3 (Fig 4E, and Appendix Fig S3E and F). In RBPJ competent cells (sh-Scr), the overexpression of L3MBTL3 leads to the strong downregulation of the *HES1* and *HEY2* Notch target genes (86 and 52% downregulation, respectively). In contrast, in RBPJ-deficient cells (sh-*RBPJ*), the overexpression of L3MBTL3 has only a mild effect on the expression of *HES1* and *HEY2* (53 and 21% downregulation, respectively; Fig 4E). These data demonstrate the RBPJ-dependent role of L3MBTL3 in the repression of Notch target genes.

To assess the extent to which L3MBTL3's ability to co-localize with RBPJ on chromatin depends on the mediation of the RBPJ/L3MBTL3 interaction by the L3MBTL3-(1-64) domain, we performed ChIP experiments to investigate chromatin binding by HA-L3MBTL3 and HA-L3MBTL3- Δ (1-64) in U87-MG cells. We observed that the occupancy of L3MBTL3 at the proximal Notch-responsive elements of Notch target genes is reduced in the absence of the RBPJ-interacting domain L3MBTL3-(1-64) (Fig 4F). Next, we tested the ability of both L3MBTL3 wild type (WT) and L3MBTL3- Δ (1-64) to repress Notch target genes in U87-MG cells. We observed that overexpression of L3MBTL3 WT downregulates some of the Notch target genes

under investigation (*HES1* and *HEY2*), validating the active role of L3MBTL3 in the repression of Notch signaling (Fig 4G). We note that the absence of effects on the expression of *HES4* and *HEY1* can be due to the presence of endogenous L3MBTL3 and the fact that these genes are already actively repressed. In contrast, not only does L3MBTL3- Δ (1-64) have no repressive effect on Notch target genes, but also its overexpression actually leads to their upregulation (Fig 4G). Thus, L3MBTL3- Δ (1-64) has a dominant negative effect on endogenous L3MBTL3's ability to repress Notch target genes. We hypothesized that this effect could be due to the "sequestration" by L3MBTL3- Δ (1-64) of co-factors that are essential for endogenous L3MBTL3 to mediate its repressive effect on Notch signaling. In the next section, we describe one such putative co-factor, KDM1A.

To validate these observations in another cell context, we tested L3MBTL3's ability to bind chromatin at the Notch-responsive elements of Notch target genes and to modulate their expression in MDA-MB-231, a human breast cancer cell line with low Notch activity (Appendix Fig S4A and B) where depletion of RBPJ results in the de-repression of Notch target genes [Appendix Fig S4C and (Kulic et al, 2015)]. In line with our observations in U87-MG cells, we

Table 1. Thermodynamic characterization of the RBPJ/L3MBTL3 interaction.

Macromolecule	Ligand	$K (M^{-1})$	$K_d (\mu\text{M})$	$\Delta G^\circ (\text{kcal/mol})$	$\Delta H^\circ (\text{kcal/mol})$	$-T\Delta S^\circ (\text{kcal/mol})$
RBPJ-(53-474)	L3MBTL3-(31-70)	$2.27 \pm 0.34 \times 10^6$	0.45 ± 0.06	-8.66 ± 0.08	-7.52 ± 0.75	1.14 ± 0.84

Calorimetric data for the binding of L3MBTL3-(31-70) to RBPJ-(53-474). All experiments were performed at 25°C. Shown are means \pm s.d. of triplicate experiments.

observed the following (i) depletion of L3MBTL3 leads to the de-repression of Notch target genes (Appendix Fig S4C); (ii) analysis of L3MBTL3 and RBPJ by ChIP-seq revealed a substantial and significant genomewide co-localization on chromatin ($P < 4 \times 10^{-57}$; two-sided Fisher exact test; Fig EV1A); (iii) genes bound by L3MBTL3 are enriched for genes associated with both the GO terms “Notch pathway genes” ($P = 4 \times 10^{-4}$) and “Notch-mediated HES/HEY network” ($P = 6 \times 10^{-5}$); (iv) L3MBTL3 co-localizes with RBPJ at the Notch-responsive elements of Notch target genes, for example, *HES1* and *HEY2* (Fig EV1B, and Appendix Fig S4D and E); (v) L3MBTL3 occupancy at the proximal Notch-responsive elements is RBPJ dependent (Appendix Fig S4E); (iii) L3MBTL3 represses Notch target genes in a RBPJ-dependent manner (Appendix Fig S4F); (iv) L3MBTL3’s ability to bind chromatin requires the presence of the RBPJ-interacting domain L3MBTL3-(1-64) (Appendix Fig S4G); and (v) L3MBTL3 repressive activity on Notch target genes is dependent on the L3MBTL3-(1-64) domain (Appendix Fig S4H). Similarly, in a clonal mouse hybridoma mature T-cell line, which is characterized by low Notch activity (Appendix Fig S5A–C), depletion of L3MBTL3 leads to the de-repression of Notch target genes (Appendix Fig S5D and E). Altogether, these data strongly support a role for L3MBTL3 in the RBPJ-dependent repression of Notch target genes in mammalian cells. Finally, in agreement with the observation that NOTCH1 ICD outcompetes L3MBTL3 for binding to RBPJ (Fig 3B and C), we note that de-repression of Notch target genes is not observed upon *L3mbtl3* knockdown in Beko cells, a mouse pre-T-cell line that is characterized by a high level of cleaved NOTCH1 ICD (Liefke et al, 2010) (Appendix Fig S5A and F).

L3MBTL3 interacts with KDM1A

L3MBTL3- Δ (1-64), the RBPJ interaction-defective mutant, has a dominant negative effect on endogenous L3MBTL3’s ability to repress Notch target genes (Fig 4G and Appendix Fig S4H). We hypothesized that this effect could be due to the “sequestration” by L3MBTL3- Δ (1-64) of co-factors that are essential for endogenous L3MBTL3 to mediate its repressive effect on gene expression. L3MBTL3 is poorly characterized at the molecular level. To identify

co-factors that may be recruited by L3MBTL3 to RBPJ-bound enhancers, we screened L3MBTL3 using our proteomic pipeline. We obtained multiple, independent lines of evidence supporting a molecular interaction between L3MBTL3 and KDM1A. First, we identified the L3MBTL3/KDM1A interaction in a Y2H screen (Fig EV2A). Second, we performed IP of endogenous RBPJ in U87-MG or MDA-MB-231 cells followed by Western blot analyses using KDM1A, L3MBTL3, or RBPJ antibody. We observed that endogenous RBPJ interacts with both endogenous KDM1A and endogenous L3MBTL3 (Fig EV2B). Third, we performed IP of V5-tagged L3MBTL3 or L3MBTL3- Δ (1-64) in U87-MG cells followed by Western blot analysis using a KDM1A antibody. We observed that endogenous KDM1A interacts with both the WT and mutant proteins (Fig EV2C).

KDM1A [lysine (K)-specific demethylase 1A] is a histone demethylase (Shi et al, 2004), which associates with different protein complexes on chromatin. Depending of the cell context, KDM1A can demethylate either the positive H3K4me1/me2 (Shi et al, 2004) or the negative H3K9me1/me2 (Metzger et al, 2005) marks and, as such, it can support either transcriptional repression or activation, respectively (Amente et al, 2013). The demethylase activity of this enzyme plays an important role in a large variety of biological processes, including development and cancer (Amente et al, 2013). Previous reports have described RBPJ-dependent recruitment of KDM1A to chromatin as an important mechanism to modulate Notch signaling in various cell contexts (Wang et al, 2007; Mulligan et al, 2011; Yatim et al, 2012). Interestingly, we observed that KDM1A also interacts with RBPJ in U87-MG cells (Fig EV2D and E).

We hypothesized that L3MBTL3 plays an essential role in the recruitment of KDM1A to RBPJ-repressor complexes. To test this hypothesis, we investigated whether the RBPJ/KDM1A interaction could be regulated in an L3MBTL3-dependent manner. In reciprocal IP experiments, we observed that both L3MBTL3 WT and L3MBTL3- Δ (1-64), the RBPJ interaction-defective mutant, co-purify with KDM1A (Figs 5A and EV2C). In the absence of L3MBTL3, the RBPJ/KDM1A interaction is weak (lane #5 in Fig 5A). Remarkably, the RBPJ/KDM1A interaction is “rescued” in the presence of L3MBTL3 WT (lane #4) but only partially rescued in the presence of

Figure 4. RBPJ recruits L3MBTL3 on chromatin to repress the expression of Notch target genes in U87-MG cells.

- A De-repression of Notch target genes upon *RBPJ* knockdown. Shown are means \pm s.d. of quadruplicate experiments. * $P < 0.05$, ** $P < 0.01$, NS, not significant; one-way ANOVA model on log-transformed data. Inset: Western blot analysis validates the shRNA-mediated depletion of RBPJ.
- B De-repression of Notch target genes in *L3MBTL3* KO U87-MG cells. Shown are means \pm s.d. of quadruplicate experiments. ** $P < 0.01$, NS, not significant; two-sample t-test on log-transformed data. Inset: Western blot analysis validates the CRISPR/Cas9-mediated KO of *L3MBTL3*.
- C RBPJ and L3MBTL3 co-localize at the proximal Notch-responsive elements of Notch target genes. Shown are means \pm s.d. of triplicate ChIP experiments.
- D L3MBTL3 occupancy at the proximal Notch-responsive elements of Notch target genes decreases upon *RBPJ* knockdown. Shown are means \pm s.d. of triplicate ChIP experiments.
- E The repressive activity of L3MBTL3 at Notch target genes is RBPJ dependent. Expression analysis of Notch target genes upon *RBPJ* knockdown and/or overexpression of L3MBTL3. Shown are means \pm s.d. of triplicate experiments. *P*-values were estimated via a one-way ANOVA model on log-transformed data where the difference of differences was tested, which is equivalent to testing the interaction in a two-way ANOVA model. Western blot analysis validates the overexpression of L3MBTL3 and the shRNA-mediated depletion of RBPJ (Appendix Fig S3E). Gene expression analyses of *OCT4* was performed as control (Appendix Fig S3F).
- F L3MBTL3 occupancy at the proximal Notch-responsive elements of Notch target genes is dependent on its RBPJ-interacting domain. ChIP analyses of HA-L3MBTL3 WT and HA-L3MBTL3- Δ (1-64) occupancy at the proximal Notch-responsive elements of Notch target genes. Shown are means \pm s.d. of duplicate experiments measured twice each.
- G The L3MBTL3-(1-64) domain is required for the downregulation of *HES1* and *HEY2* in U87-MG cells. Expression analysis of Notch target genes upon overexpression of L3MBTL3 WT, L3MBTL3- Δ (1-64), or LacZ control (Control). Shown are means \pm s.d. of triplicate experiments. * $P < 0.05$, ** $P < 0.01$, NS, not significant; one-way ANOVA model on log-transformed data.

Data information: In panels (C, D, and F): distance in base pairs (bp) relative to the transcriptional start site (TSS) is indicated below the gene names. Chrom8 was used as negative control (NEG).

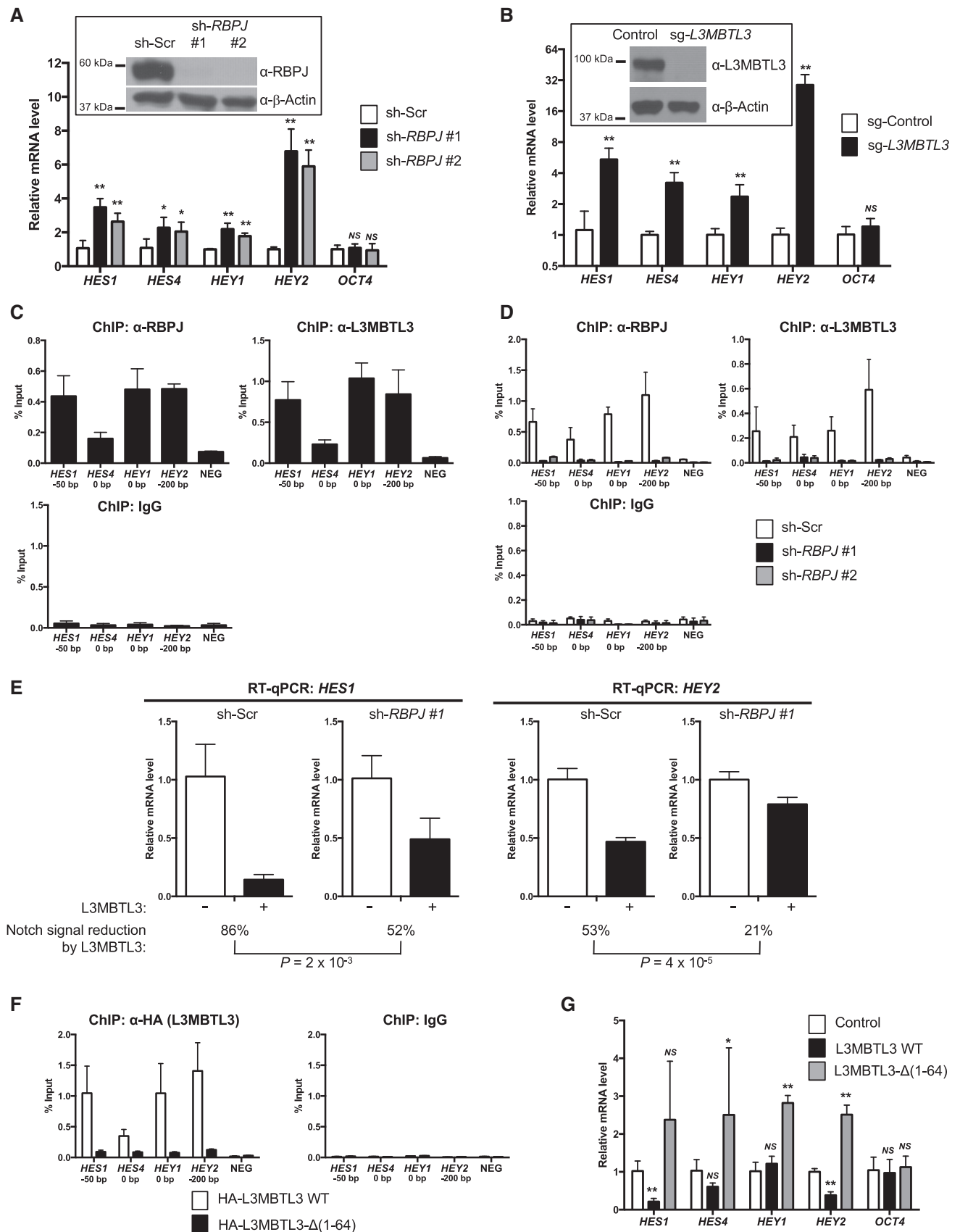


Figure 4.

L3MBTL3-Δ(1-64) (lane #6), suggesting that the previously reported RBPJ/KDM1A interaction is indirect and occurs via L3MBTL3.

L3MBTL3 recruits KDM1A at RBPJ-bound sites

We hypothesized that L3MBTL3 mediates the recruitment of KDM1A to RBPJ-bound sites. To test this hypothesis, we investigated KDM1A occupancy at the Notch-responsive elements of Notch target genes in *L3MBTL3* KO U87-MG cells by ChIP. We observed that KDM1A occupancy is strongly reduced at the proximal Notch-responsive elements of Notch target genes in the absence of L3MBTL3 (Fig 5B). The L3MBTL3-dependent KDM1A occupancy at these sites can be efficiently rescued by overexpression of L3MBTL3 WT (Fig 5C). In contrast, upon overexpression of either L3MBTL3-Δ(1-64), the RBPJ interaction-defective mutant (Fig 2B), or L3MBTL3-Δ(SAM), a KDM1A interaction-defective mutant (Fig EV2F), KDM1A occupancy at these proximal Notch-responsive elements remains partially [L3MBTL3-Δ(1-64)] or completely [L3MBTL3-Δ(SAM)] impaired (Fig 5C). Altogether, our results demonstrate that L3MBTL3 links KDM1A to RBPJ at Notch-responsive elements.

L3MBTL3 represses Notch target genes via KDM1A

Methylation of H3K4 is linked to transcriptional activation (Noma et al, 2001). Yatim et al (2012) previously described that KDM1A contributes to the RBPJ-mediated repression of Notch target genes via demethylation of H3K4me2 in U937, a myeloid cell line characterized by low Notch signaling tone. Similarly, in U87-MG cells, we observed that de-repression of Notch target genes upon *RBPJ* knockdown (Fig 4A) is associated with a significant increase in H3K4me2 (Appendix Fig S6A). We hypothesized that L3MBTL3 represses Notch target genes by promoting the KDM1A-mediated demethylation of H3K4me2. To test this hypothesis, we performed gene expression and ChIP analyses of the well-characterized Notch target gene *HES1* upon overexpression of L3MBTL3 WT, L3MBTL3-Δ(1-64), or L3MBTL3-Δ(SAM). We observed that H3K4me2 decreases considerably upon overexpression of L3MBTL3 WT (Fig 5D and Appendix Fig S6B). In contrast, H3K4me2 remains stable upon

overexpression of L3MBTL3-Δ(1-64) and decreases more mildly upon overexpression of L3MBTL3-Δ(SAM) (Fig 5D). Accordingly, the expression of *HES1* decreases considerably upon overexpression of L3MBTL3 WT but not of either L3MBTL3-Δ(1-64) or L3MBTL3-Δ(SAM) (Fig 5E). Thus, L3MBTL3 promotes the repression of *HES1* via KDM1A-mediated demethylation of H3K4me2.

dL(3)mbt genetically interacts with Notch in *Drosophila*

Drosophila is the model system of choice to study Notch signaling *in vivo* (Kopan & Ilagan, 2009; Guruharsha et al, 2012). In *Drosophila*, the Notch pathway governs numerous cell fate decisions throughout morphogenesis (Bray, 2006; Guruharsha et al, 2012) and it has a profound effect on many aspects of nervous system development, including the formation of neuroblasts from neuroepithelial cells (Egger et al, 2010; Reddy et al, 2010; Yasugi et al, 2010). Interestingly, *dL(3)mbt*, the fly homolog of the human *L3MBTL3* gene, was originally discovered in *Drosophila* where it behaves as a suppressor of brain tumorigenesis in the larval optic lobe (Wismar et al, 1995; Richter et al, 2011). Moreover, in a combined *ex vivo* and *in vivo* RNAi screen for Notch regulators in *Drosophila*, the RNAi-mediated knockdown of *dL(3)mbt* leads to the upregulation of Notch signaling (Saj et al, 2010). These observations support the hypothesis of a functional link between the Notch pathway and *dL(3)mbt* in *Drosophila*.

We sought to further investigate the interaction between the Notch pathway and *dL(3)mbt* using a combination of computational, molecular, and genetic approaches (Figs 6, and EV3 and EV4, and Appendix Figs S7–S12). Using a hidden Markov model (HMM) approach to detect protein homology (Soding, 2005), HMM profile–profile alignment analyses identified a conserved region between the RBPJ-interacting domain L3MBTL3-Δ(1-64) (exact amino acid position of the conserved region is Q11-N50) and a region of the *Drosophila* *dL(3)mbt* protein (amino acid position S658-Q698) ($P = 6 \times 10^{-19}$; Fig EV3). Accordingly, in a GST pulldown assay, we observed that *dL(3)mbt* directly interacts with Su(H), the *Drosophila* homolog of RBPJ (Fig 6A). Furthermore, the analysis of previously published ChIP-chip and ChIP-seq data for Su(H) (Zacharioudaki

Figure 5. L3MBTL3 recruits KDM1A at RBPJ-bound Notch-responsive elements to repress Notch target genes.

- A The RBPJ/KDM1A interaction is indirect and occurs via L3MBTL3. IP of HA-KDM1A in the presence of overexpressed V5-L3MBTL3 or V5-L3MBTL3-Δ(1-64) in *L3MBTL3* KO U87-MG cells. CRISPR/Cas9 sg-*L3MBTL3*-resistant plasmids were used to overexpress the L3MBTL3 proteins. The experiment was independently replicated twice.
- B KDM1A occupancy at the proximal Notch-responsive elements of Notch target genes is L3MBTL3 dependent. ChIP analysis of endogenous KDM1A in *L3MBTL3* KO U87-MG cells. Shown are means ± s.d. of duplicate experiments measured twice each.
- C KDM1A occupancy at the proximal Notch-responsive elements of Notch target genes is dependent on L3MBTL3, and both its RBPJ interaction and KDM1A interaction domains. ChIP analysis of endogenous KDM1A in *L3MBTL3* KO U87-MG cells upon overexpression of L3MBTL3, L3MBTL3-Δ(1-64) or L3MBTL3-Δ(SAM). Control: empty vector. Shown are means ± s.d. of duplicate experiments measured twice each.
- D L3MBTL3, but neither L3MBTL3-Δ(1-64) nor L3MBTL3-Δ(SAM), leads to decreasing H3K4me2 at the proximal Notch-responsive element of *HES1*. ChIP analysis of H3K4me2 at the proximal Notch-responsive element of *HES1* upon overexpression of LacZ control (Control), L3MBTL3, L3MBTL3-Δ(1-64), or L3MBTL3-Δ(SAM) in *L3MBTL3* KO U87-MG cells. Shown are means ± s.d. of duplicate experiments measured twice each. *P*-values were estimated via a one-way ANOVA on log-transformed data.
- E L3MBTL3, but neither L3MBTL3-Δ(1-64) nor L3MBTL3-Δ(SAM), represses *HES1*. Expression analysis of *HES1* upon overexpression of LacZ control (Control), L3MBTL3, L3MBTL3-Δ(1-64), or L3MBTL3-Δ(SAM) mutants in *L3MBTL3* KO U87-MG cells. Shown are means ± s.d. of triplicate experiments. *P*-values were estimated via a one-way ANOVA on log-transformed data. *NS*, not significant. WB, Western blot; IP, immuno-precipitation. We note that in the context of this experiment, that is, in the absence of endogenous L3MBTL3, the overexpression of L3MBTL3-Δ(1-64) does not result in the increased expression of *HES1*, contrasting with the result obtained in Fig 4G, that is, in the presence of endogenous L3MBTL3. Indeed, as expected, the dominant negative effect of L3MBTL3-Δ(1-64) on endogenous WT L3MBTL3's ability to repress the expression of Notch target genes can only be observed when WT L3MBTL3 is expressed.

Data information: Panels (B–D): distance in bp relative to the TSS is indicated below the gene names. Chrom8 was used as negative control (NEG). Source data are available online for this figure.

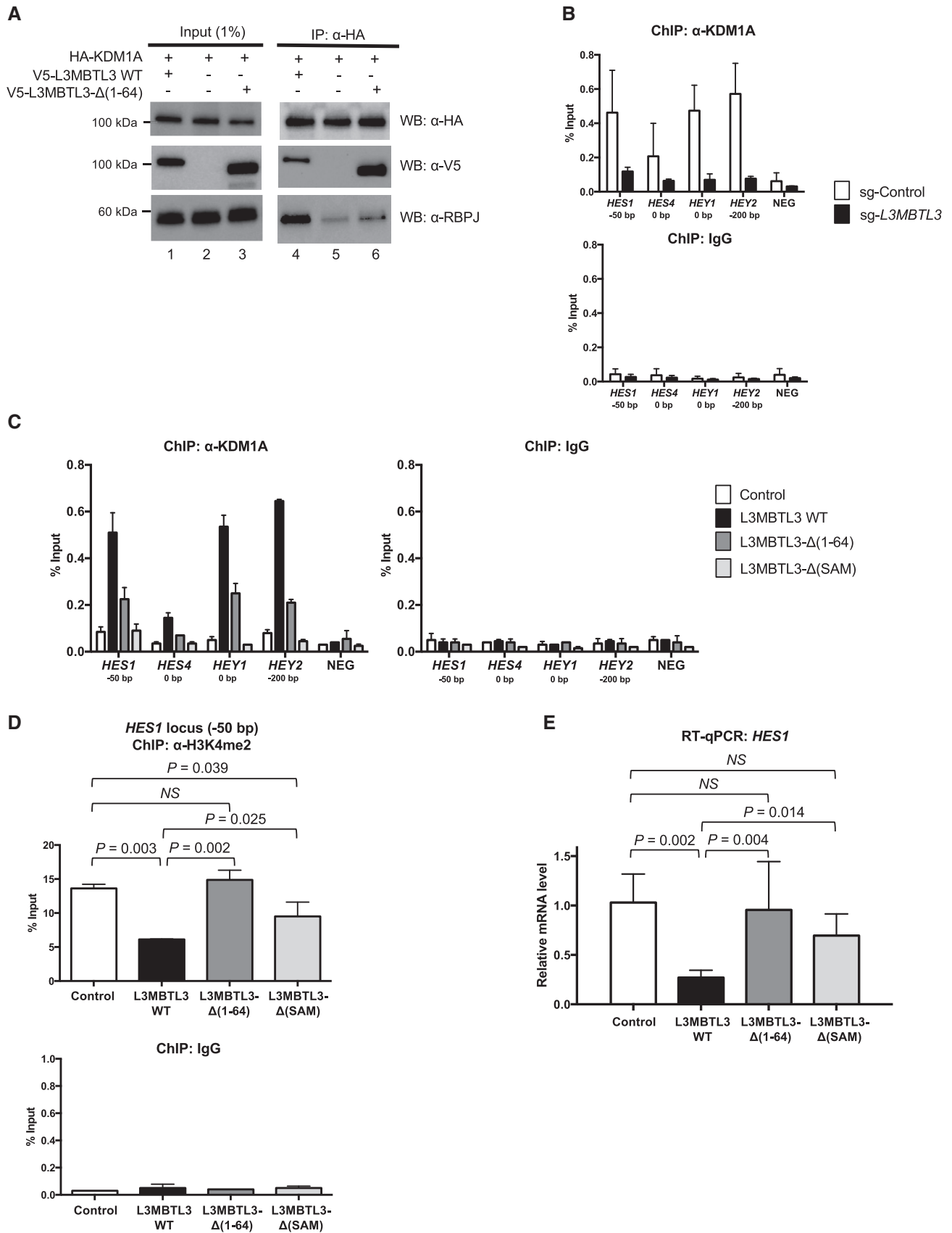


Figure 5.

Figure 6. The interaction between RBPJ/Su(H)/lag-1 and L3MBTL3/dL(3)mbt/lin-61 is evolutionarily conserved.

- A GST pull-down showing that dL(3)mbt, the *Drosophila* homolog of L3MBTL3, directly interacts with Su(H), the *Drosophila* homolog of RBPJ. *In vitro*-transcribed and translated dL(3)mbt or dNotch ICD (dNotch ICD fragment containing the RAM domain and ANK repeats), as positive control, was incubated with bacterially purified GST-Su(H) or GST alone pre-bound to GSH beads. Proteins were resolved via SDS-PAGE and signals were acquired via X-ray exposure. The experiment was independently replicated four times.
- B dL(3)mbt and Su(H) co-localize genomewide. Venn diagram showing the genomewide co-localization of dL(3)mbt and Su(H).
- C Snapshot showing the co-localization of dL(3)mbt and Su(H) at the *dNotch* (*N*) locus.
- D In the wing imaginal disk, dL(3)mbt overexpression in the dorso-ventral (D-V) boundary results in the downregulation of the Notch target gene *cut*. Wing disks expressing *UAS-GFP* (top panels) or *UAS-HA-dL(3)mbt;UAS-GFP* (bottom panels) under the *ug-Gal4* driver at 25°C were stained for cut and HA. GFP marks the *ug-Gal4* expression domain. Insets below each panel show a closer view of the D-V boundary with yellow arrows marking the regions where HA-dL(3)mbt is expressed and cut is downregulated. At least 20 disks for each genotype were analyzed. Representative images are shown. Scale bars: 100 μm.
- E The *ug-Gal4*-driven HA-dL(3)mbt overexpression causes a serrated wing (wing notching) phenotype. Flies expressing either *UAS-GFP* or *UAS-HA-dL(3)mbt;UAS-GFP* under *ug-Gal4* were reared to adulthood at 25°C. *P*-values were estimated by comparing the proportions via a two-proportion Z-test. Scale bars: 200 μm.
- F Functional interaction between *lag-1/RBPJ* and *lin-61/L3MBTL3* during *Caenorhabditis elegans* vulva development. Proportion of animals ($n \geq 100$) displaying a protruding vulva (Pvl) phenotype after RNAi treatment for two generations. Worms were grown at 25°C. Shown are means \pm s.d. of duplicate experiments. EV, empty vector control.

et al, 2016) and dL(3)mbt (Li *et al*, 2015a) revealed a substantial and significant genomewide co-localization of the proteins under investigation ($P < 1 \times 10^{-31}$; two-sided Fisher exact test; Fig 6B). Among the co-bound sites, we note the presence of “classical” *Drosophila* Notch targets, for example, the *E(spl)* locus, *lola*, and *dNotch* itself (Fig 6C and Appendix Fig S7). In a complementary analysis of mRNA expression and in agreement with the observation that the RNAi-mediated knockdown of *dL(3)mbt* leads to the upregulation of Notch signaling (Saj *et al*, 2010), we observed that genes identified as upregulated in brain tumors upon *dL(3)mbt* KO (Janic *et al*, 2010) overlap with genes identified as upregulated in brain tumors upon sustained NICD expression (Zacharioudaki *et al*, 2016) ($P = 0.01$; two-sided Fisher exact test), indicating that both types of brain tumors share a common expression signature.

To investigate the *in vivo* relevance of the Su(H)/dL(3)mbt interaction, we examined the functional cross talk between the Notch pathway and dL(3)mbt in various *Drosophila* tissues. First, we observed that the *E(spl)mγ-HLH-GFP* reporter is upregulated in larval brain tumors induced by loss of *dL(3)mbt* (Appendix Fig S8). Second, expression of dL(3)mbt suppresses dNICD-induced hyperplasia in the eye imaginal disk (Fig EV4). Accordingly, the combined loss of function of *dL(3)mbt* and gain of function of *dNICD* synergize to promote hyperplasia in the eye imaginal disk (Appendix Fig S9). The disk cells at the dorsal-ventral compartment border generate the wing margin, and loss of wing margin cells (wing notching) is one of the characteristic phenotypes associated with loss of Notch signaling, for example, *Notch* haploinsufficiency (Morgan, 1917). Remarkably, we observed that the exogenous expression of dL(3)mbt is not only associated with the repression of the Notch target gene *cut* in the wing disk (Fig 6D and Appendix Figs S10–S12), and it also results in the classic wing notching phenotype in adult flies (Fig 6E). Altogether, these data suggest that *dL(3)mbt* is a *bona fide* regulator of the Notch pathway and underscore a striking conservation of the Notch pathway/L3MBTL3 interaction from insects to mammals.

lag-1 genetically interacts with lin-61 in *Caenorhabditis elegans*

Genetic analysis of Notch signaling in *C. elegans* has illuminated universal aspects of this essential and conserved pathway (Greenwald, 2012), for example, establishing the requirement of the

γ -secretase complex for Notch signal activation (Levitani & Greenwald, 1995). To further explore the functional relevance of the/L3MBTL3 interaction across species, we sought to investigate the functional link between *lag-1* and *lin-61*, the *C. elegans* homologs of *RBPJ* and *L3MBTL3* genes, respectively. The role of Notch signaling in mediating cell–cell interactions is essential throughout *C. elegans* morphogenesis and is particularly well documented in embryonic (Priess, 2005) and vulva development (Gupta *et al*, 2012). Interestingly, independent genetic and expression studies have linked both *lag-1* and *lin-61* to both these developmental processes (Qiao *et al*, 1995; Rual *et al*, 2004; Harrison *et al*, 2007). These observations prompted us to investigate the functional cross talk between *lag-1* and *lin-61* during embryogenesis and vulva development.

During embryogenesis, a proportion of the *lag-1(om13)* thermosensitive mutant embryos fail to develop and do not hatch (Qiao *et al*, 1995). In N2 animals (N2 refers to the WT strain), we observed that the RNAi-induced inactivation of *lin-61* has no incidence on embryonic lethality (Fig EV5). In contrast, in *lag-1(om13)* animals, *lin-61(RNAi)* results in a twofold increase of embryonic lethality from 27 to 51%, thus demonstrating a genetic interaction between *lag-1* and *lin-61* during *C. elegans* embryonic development (Fig EV5). Furthermore, during vulva development, we observed that ~19% of *lag-1(RNAi)* animals and ~11% of *lin-61(n3809)* mutants present a protruding vulva phenotype (Pvl), compared to only ~2% for the control (N2) animals. Interestingly, the combined inactivation of *lag-1* and *lin-61* [*lag-1(RNAi); lin-61(n3809)*] resulted in a synergistic effect, that is, 52% of the animals show a Pvl phenotype, indicating a functional interaction between *lag-1* and *lin-61* (Fig 6F). Remarkably, a functional link between *RBPJ/Su(H)/lag-1* and *L3MBTL3/dL(3)mbt/lin-61* (human/fly/worm) is thus conserved across metazoan species (Figs 6 and EV3–EV5, and Appendix Figs S7–S12).

Discussion

Our molecular studies demonstrate a direct, physical interaction between RBPJ and L3MBTL3. Our mapping and thermodynamic studies revealed that the interaction is mediated by the L3MBTL3-(31-70) and the RBPJ-BTD domains with a 450 nM binding affinity. The RBPJ-BTD domain also interacts with the NOTCH ICD-RAM

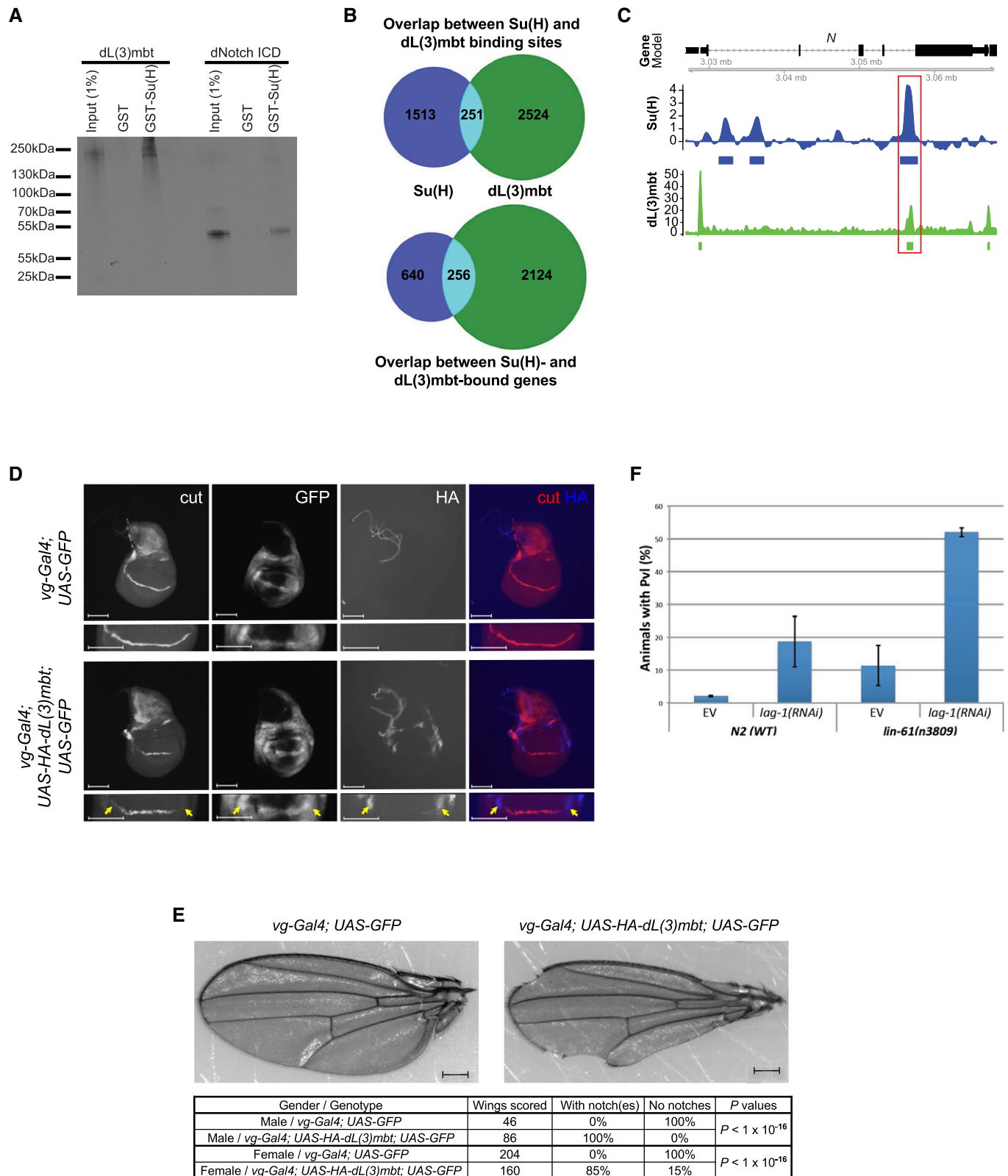


Figure 6.

domain and is required for the formation of the NTC (Kopan & Ilagan, 2009). As suggested by the moderate binding strength of the RBPJ/L3MBTL3 interaction, which is 20-fold weaker than the

affinity of the RBPJ/NOTCH ICD-*RAM* interaction (Friedmann *et al*, 2008), and by the observation that both L3MBTL3 and NOTCH ICD interact with the *BTD* domain of RBPJ, we observed that NOTCH

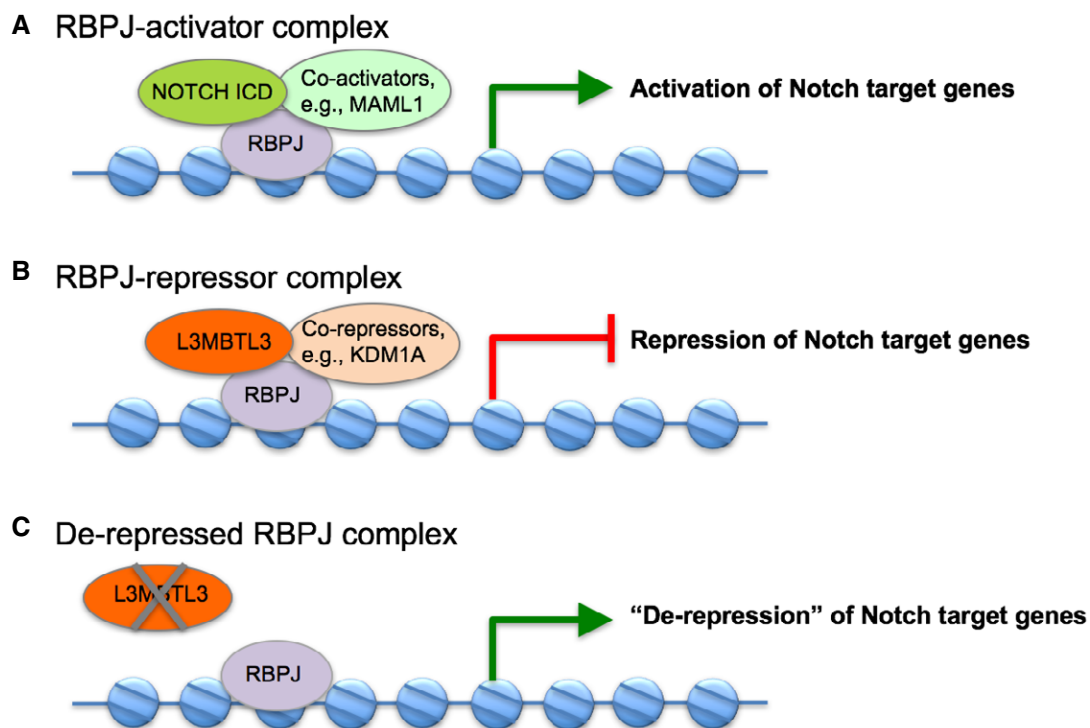


Figure 7. Model for the regulation of Notch target genes by L3MBTL3.

- A NOTCH ICD binds to RBPJ-bound Notch-responsive elements where it builds up a co-activator complex composed of Mastermind-like 1 (MAML1) and additional co-activators to induce expression of Notch target genes.
- B In the absence of Notch signaling, L3MBTL3 interacts with RBPJ at Notch-responsive elements where it recruits KDM1A to repress Notch target genes.
- C Loss of function of L3MBTL3 leads to de-repression of Notch target genes.

ICD outcompetes L3MBTL3 for binding to RBPJ. Other RBPJ co-factors, for example, EBNA2 and KyoT2, have been previously shown to interact with RBPJ through "RAM-like" domains (Ling & Hayward, 1995; Collins *et al*, 2014) which, as the NOTCH ICD-RAM domain, are characterized by a $\phi W\phi P$ (ϕ = hydrophobic) tetrapeptide motif (Kovall & Hendrickson, 2004). As observed for the other RBPJ co-factor MINT, there are no such RAM-like domains detectable in the L3MBTL3 amino acid sequence, suggesting that a different interaction motif is involved.

Malignant brain tumor domain-containing proteins have been linked to transcriptional repression across metazoans (Harrison *et al*, 2007; Trojer *et al*, 2007; Grimm *et al*, 2009; Bonasio *et al*, 2010; Richter *et al*, 2011; Tang *et al*, 2013), but it remains unclear how they are recruited to specific regions of the genome. There are only a few reports where models of recruitment mechanisms have been proposed (Bocconi *et al*, 2003; Tang *et al*, 2013). Is L3MBTL3, which, of all MBT proteins, appears to have the lowest selectivity for any particular methylated histone mark (Nady *et al*, 2012), bound to chromatin? Our data provide clear support for the RBPJ-mediated recruitment of L3MBTL3 to chromatin at the Notch-responsive elements of Notch target genes. The role of the MBT and ZnF domains in this context remains to be characterized. Finally, in agreement with the well-documented role of MBT proteins as chromatin condensers (Bonasio *et al*, 2010) and the fact that NOTCH ICD and L3MBTL3 compete for binding to RBPJ, our expression analysis of Notch target genes shows that L3MBTL3 is a negative

regulator of Notch signaling in mammalian cells. The observation that NOTCH ICD displaces L3MBTL3 from RBPJ suggests that the functional relevance of L3MBTL3 to the regulation of Notch target genes may be particularly important in cell contexts where the DSL ligand-dependent activation of Notch and subsequent release of NOTCH ICD are low or moderate.

The recruitment of KDM1A by RBPJ to chromatin has been previously linked to the modulation of Notch signaling (Wang *et al*, 2007; Mulligan *et al*, 2011; Yatim *et al*, 2012). We have now expanded these observations by further dissecting the molecular mechanism that governs KDM1A recruitment at Notch-responsive elements. Our results unveil L3MBTL3 as a key molecular link between RBPJ and KDM1A in RBPJ-repressive complexes and indicate that the repressive role of L3MBTL3 at Notch target genes is mediated through the KDM1A-dependent demethylation of H3K4me2. We propose a molecular model in which L3MBTL3 recruits KDM1A at RBPJ-bound sites and promotes the repression of Notch signals via KDM1A-dependent H3K4me2 demethylation (Fig 7). Interestingly, L3MBTL3 has the highest affinity toward dimethylated marks, including H3K4me2, though relatively promiscuous (Nady *et al*, 2012). We speculate that, during the transition of RBPJ-bound Notch-responsive elements from the "ON" to the "OFF" state, the preferential binding of L3MBTL3 to H3K4me2 may contribute to the preferential recruitment of KDM1A at sites where KDM1A's H3K4me2 demethylase activity is most needed to negatively regulate the chromatin landscape, that is, at the hitherto

active, yet-to-be inactivated, H3K4me2-rich RBPJ-bound sites. As such, the L3MBTL3/KDM1A interaction may play a crucial role in the early transition of RBPJ-bound sites from the active to the repressed state.

Our results, together with previously reported observations, support the hypothesis that our molecular model is conserved in *Drosophila*. First, dL(3)mbt and Su(H) interact with each other and co-localize at Notch target genes. Second, dL(3)mbt represses reporters of Notch activity and Notch target genes [also observed in (Saj *et al*, 2010)]. Third, both *Notch* and *dL(3)mbt* mediate critical developmental function in the same tissue, that is, neurogenesis in the optic lobe (Wismar *et al*, 1995; Egger *et al*, 2010; Reddy *et al*, 2010; Yasugi *et al*, 2010; Richter *et al*, 2011). Fourth, *Notch* and *dL(3)mbt* interact genetically to control cell fate in the eye imaginal disk. Fifth, dL(3)mbt overexpression causes a serrated wing (wing notching) phenotype. Sixth, dL(3)mbt co-purifies with PF1, a PHD-finger protein that was previously linked to Notch signaling (Moshkin *et al*, 2009). It remains to be investigated whether PF1 regulates Notch signaling as part of a dL(3)mbt-containing complex and/or as part of a complex containing ASF1 and the H3K4me2/3 demethylase LID (Goodfellow *et al*, 2007; Moshkin *et al*, 2009). Last but not least, we note that *Su(var)3-3*, the fly homolog of KDM1A, genetically interacts with the Notch signaling pathway and also has a dual role in modulating Notch signaling in *Drosophila* (Di Stefano *et al*, 2011). Moreover, the dL(3)mbt and Su(var)3-3 proteins co-purify in LINT complexes isolated from third-instar larval brains (Meier *et al*, 2012). Altogether, these observations support a model in which *dL(3)mbt* represses Notch signaling in *Drosophila*. It also suggests a striking conservation of the Notch pathway/dL(3)mbt/Su(var)3-3 interaction from insects to mammals. Further studies are required to characterize the molecular mechanisms in which Su(H), dL(3)mbt, and Su(var)3-3 are involved on chromatin and to assess whether *Su(var)3-3*'s ability to regulate Notch signaling depends on *dL(3)mbt*.

To further explore the functional *in vivo* relevance of the RBPJ/L3MBTL3 interaction in metazoans, we studied in *C. elegans* the link between *lag-1* and *lin-61*, the worm homologs of the RBPJ and L3MBTL3 genes, respectively. Our results indicate that both genes interact genetically during both embryonic and vulva development. In *C. elegans*, *spr-5* encodes an H3K4me2 demethylase homologous to KDM1A. Remarkably, *spr-5* was originally discovered in a genetic screen as a suppressor of the egg-laying defective phenotype of *sel-12* (Jarriault & Greenwald, 2002); indeed, the product of *sel-12* is a key component of the γ -secretase complex and the key role of this complex for Notch signal activation was originally established in *C. elegans* using a genetic approach (Levitan & Greenwald, 1995). In one of their models, Jarriault and Greenwald speculate that SPR-5 contributes to the repression of Notch target genes by forming a repressor complex with LAG-1 in the absence of Notch activation (Jarriault & Greenwald, 2002), mirroring our RBPJ/L3MBTL3/KDM1A model (Fig 7).

In conclusion, we identified a previously uncharacterized RBPJ interactor, L3MBTL3, which contributes to the repression of Notch target genes via KDM1A-dependent histone H3K4 demethylation. Our *in vivo* data in *Drosophila* and *C. elegans* demonstrate that the functional link between RBPJ and L3MBTL3 is evolutionarily conserved, thus identifying L3MBTL3 as a universal modulator of Notch target genes in metazoans.

Materials and Methods

Appendix Supplementary Methods can be found in the Appendix file.

Yeast two-hybrid (Y2H)

Yeast two-hybrid (Y2H) screens were performed as previously described (Dreze *et al*, 2010).

Affinity purification coupled to mass spectrometry analysis

U87-MG cells transfected with pcDNA3-HA-DEST encoding RBPJ, L3MBTL3, or EGFP control were collected, washed with ice-cold PBS, and lysed in ice-cold lysis buffer [50 mM Tris pH 7.8, 150 mM NaCl, 0.5% NP-40, 10% glycerol, 2 mM NaF, 2 mM Na₃VO₄, and Complete[®] protease inhibitor (1× final, Roche[®], 05 056 489 001)]. HA-tagged proteins were affinity-purified with 50 μ l of α -HA agarose beads (Sigma[®], A2095) at 4°C for 2 h with rotation. Beads were washed four times with lysis buffer, three times with washing buffer (50 mM Tris pH 7.8, 100 mM NaCl, 0.1% NP-40), and three times with 50 mM NH₄HCO₃. Proteins were eluted twice with 50 μ l of 1% ammonia (NH₄OH; Sigma[®], 338818), dried, and resuspended in 20 μ l Laemmli sample buffer. Proteins were resolved via SDS-PAGE and the whole gel lanes were cut into five pieces that were individually subjected to in-gel tryptic digestion, as previously described (Shevchenko *et al*, 2006). Peptides were dried and analyzed via LC-MS/MS system, as follows.

Peptides were resolved on a nano-capillary reverse phase column (PicoFrit column, New Objective[®]) using a 5–50% acetonitrile gradient at 300 nl/min and directly introduced into an ion-trap mass spectrometer (LTQ XL, Thermo Fisher[®]). Data-dependent MS/MS spectra on the five most intense ions from each full MS scan were collected (relative collision energy ~35%). Proteins were identified by searching the data against Swiss-Prot human database (January 9th 2013) appended with decoy (reverse) sequences using the X! Tandem/Trans-Proteomic Pipeline software suite (Pedrioli, 2010). All peptides and proteins with a PeptideProphet (Keller *et al*, 2002) and ProteinProphet (Nesvizhskii *et al*, 2003) probability score of >0.8 (false discovery rate < 2% estimated using a target-decoy strategy) were considered positive identifications. Proteins were considered potential RBPJ interactors if they were identified with two or more mass spectra in both duplicate RBPJ AP-MS experiments but not in the EGFP-negative AP-MS control experiments. Proteins identified in > 10% of the AP-MS experiments available in the CRAPome database version 1.1, a contaminant repository for AP-MS data (Mellacheruvu *et al*, 2013), were considered background contaminants and removed from the analysis. The mass spectrometry proteomics data have been deposited to the ProteomeXchange Consortium via the PRIDE (Vizcaino *et al*, 2016) partner repository with the dataset identifier PXD004196.

Isothermal titration calorimetry

Isothermal titration calorimetry experiments were carried out using a MicroCal VP-ITC microcalorimeter. All experiments were performed at 25°C in a buffer composed of 50 mM sodium phosphate pH 6.5 and 150 mM NaCl. Purified RBPJ core domain (53–474) and L3MBTL3 (31–70) proteins were degassed and buffer-matched using

size exclusion chromatography. Experiments were carried out with 10–20 μ M RBPJ in the cell and 100–200 μ M L3MBTL3 in the syringe. Raw data were normalized to the corresponding L3MBTL3 heat of dilution and fit to a one-site binding model using the ORIGIN software. The following proteins were used: human L3MBTL3-(31-70) (accession #KJ899798) and mouse RBPJ-(53-474) (accession #P31266.1).

Chromatin immuno-precipitation (ChIP)

Cells were fixed for 15 min at room temperature with 1% paraformaldehyde added directly to the medium, washed twice with ice-cold PBS, and snap-frozen on dry ice. Cells were then lysed in SDS lysis buffer (1% SDS, 10 mM EDTA, 50 mM Tris-HCl pH 8.0), sheared through a 27-gauge needle, and sonicated. Samples were centrifuged for 20 min at 13,000 g, and the supernatant was diluted at a 1:10 ratio with dilution buffer (0.01% SDS, 1% Triton X-100, 1.2 mM EDTA, 16.7 mM Tris-HCl pH 7.5, 167 mM NaCl). Chromatin was incubated with 2.5 μ g of the desired antibody overnight at 4°C with rotation. Immuno-complexes were captured with 30 μ l of BSA-preblocked protein G Dynabeads (Invitrogen[®], 10009D) for 1 h at 4°C with rotation. Beads were washed once in low-salt (150 mM NaCl, 2 mM EDTA, 0.1% SDS, 1% Triton X-100, 20 mM Tris-HCl pH 7.5), once in high-salt (500 mM NaCl, 2 mM EDTA, 0.1% SDS, 1% Triton X-100, 20 mM Tris-HCl pH 7.5), once in lithium chloride (25 mM LiCl, 1% NP40, 1% Deoxycholic Acid, 1 mM EDTA, 10 mM Tris-HCl pH 7.5), and twice with TE (10 mM Tris-HCl pH 7.5, 1 mM EDTA) buffers for 5 min each. Chromatin was eluted in 250 μ l of elution buffer (1% SDS, 100 mM NaHCO₃) for 30 min at 42°C, and cross-linking was reversed by overnight incubation at 65°C in presence of 50 mM (final concentration) NaCl. Samples were incubated with RNase A (Qiagen[®], 19101), and DNA was purified using the Qiagen[®] PCR purification kit (Qiagen[®], 28106). Samples were analyzed via quantitative PCR (qPCR) using the Power SYBR Green PCR master mix (Applied Biosystems[®], 4367662) and the CFX96 Touch™ Real-Time PCR Detection System (Bio-Rad[®]) according to manufacturer's recommendations. Primers used in ChIP experiments are listed in Table EV2 and their genome location is shown in Appendix Fig S3A. A region of chromosome 8 (Chr8:127010162 + 127010260) was used as negative control (NEG).

Gene expression analyses

Total RNA was extracted with TRIzol reagent (Ambion[®], 15596018) according to manufacturer's instructions and further purified with the RNeasy Mini Kit (Qiagen[®], 74106). Five micrograms of RNA was retro-transcribed in cDNA using oligo(dT)18-primed reverse transcription and SuperScript III RT First-Strand kit (Invitrogen[®], 18080-051) as described by the manufacturer. The cDNA was analyzed via qPCR analysis using the Power SYBR Green PCR master mix (Applied Biosystems[®], 4367662) and the CFX96 Touch™ Real-Time PCR Detection System (Bio-Rad[®]) according to manufacturer's recommendations. Data were normalized to the reference gene glyceraldehyde 3-phosphate dehydrogenase (GAPDH). For gene expression analyses in mature T cells, 1 μ g of RNA was retro-transcribed in cDNA using random hexamers and M-MuLV reverse transcriptase (NEB[®]). qPCRs were assembled with Absolute QPCR

ROX Mix (Thermo Scientific[®], AB-1139), gene-specific oligonucleotides, and double-dye probes and analyzed using the StepOne-Plus Real-Time PCR System (Applied Biosystem[®]). Data were normalized to the reference gene hypoxanthine-guanine phosphoribosyltransferase (HPRT). Primers used in RT-qPCR experiments are listed in Table EV2.

Hidden Markov model profile alignment analyses

Hidden Markov model profile alignment analyses were performed as previously described (Soding, 2005).

Drosophila melanogaster

All *Drosophila* stocks were maintained under standard conditions at 25°C unless otherwise stated. *dL(3)mbt*^{GM76}, a temperature-sensitive hypomorphic allele of *dL(3)mbt*, was generously provided by Dr. R. Lehmann (Yohn *et al*, 2003). In Appendix Fig S8, the *dL(3)mbt*^{GM76} mutant is in heterozygosity with *Df(3R)D605*, a *dL(3)mbt* deficiency line in which the whole *dL(3)mbt* locus is deleted. *Df(3R)D605* was obtained from Bloomington *Drosophila* Stock Center at Indiana University, Bloomington, Indiana (Stock #823). The *UAS-HA-dL(3)mbt* transgene was generated following a standard *P-element*-mediated germline transformation. The *E(spl)mγ-GFP* transgenic line (Almeida & Bray, 2005) was kindly provided by Dr. S. Bray. The *UAS-dNICD* line was previously described (Go *et al*, 1998). The *UAS-GFP* and *UAS-p35* lines were obtained from the Bloomington *Drosophila* Stock Center at Indiana University, Bloomington, Indiana (Stock #1521 and #5073, respectively). The expression of the *UAS*-dependent transgenes was driven by *E1-Gal4* (Pallavi *et al*, 2012), *vg-Gal4* (Bloomington *Drosophila* Stock Center #6819), or *ptc-Gal4* (Bloomington *Drosophila* Stock Center #2017). For Fig EV4A–P, *E1-Gal4* and *UAS-dNICD/CyO,tub-Gal80;E1-Gal4* virgin females were crossed to *UAS-HA-dL(3)mbt/CyO-Tb* or *w¹¹¹⁸* males. For Fig EV4Q–T, *UAS-HA-dL(3)mbt/CyO-Tb* virgin females were crossed to *UAS-dNICD/CyO,tub-Gal80;E1-Gal4* or *UAS-GFP;E1-Gal4* males, *UAS-dNICD/CyO-Tb virgin females to UAS-GFP;E1-Gal4* males, and *UAS-GFP virgin females to UAS-GFP;E1-Gal4* males. To investigate the combined loss of *dL(3)mbt* together with *dNICD* in the eye imaginal disks, *UAS-GFP/CyO,GFP;dL(3)mbt^{GM76}/TM6B,Tb¹*, *UAS-dNICD/CyO,GFP;dL(3)mbt^{GM76}/TM6B,Tb¹*, or *UAS-dNICD* males were crossed with *E1-Gal4* virgin females at non-permissive temperature (31°C). For Fig 6D and E, *vg-Gal4/CyO;UAS-GFP* virgin females were crossed to *UAS-HA-dL(3)mbt/CyO-Tb* or *w¹¹¹⁸* males. For Appendix Fig S11, *UAS-dNICD(X);vg-Gal4/CyO;UAS-GFP/TM6B,Tb¹,tub-Gal80* males were crossed to *UAS-HA-dL(3)mbt/CyO-Tb* or *UAS-GFP* virgin females and only female progeny (containing *UAS-dNICD*) were collected. *Ptc-Gal4* experiments were performed by crossing *ptc-Gal4;tub-Gal80^{ts}/CyO-TM6B,Tb¹* virgin females to *UAS-HA-dL(3)mbt/CyO;UAS-GFP/TM6B,Tb¹*, *UAS-dNICD*, *UAS-HA-dL(3)mbt/CyO;UAS-dNICD*, or *w¹¹¹⁸* males; crosses were maintained at 18°C (permissive temperature for *Gal80^{ts}*) and transferred to 31°C (restrictive temperature) for 26 h prior to harvesting.

Staining of eye disks was performed from third-instar larvae as follows: eye disks were dissected in PBS, fixed in PLP buffer (2% paraformaldehyde, 10 mM NaIO₄, 75 mM lysine, 37 mM sodium phosphate, pH 7.2) or 3.7% formaldehyde in 1× PBS, washed in PBS-DT (0.3% sodium deoxycholate, 0.3% Triton X-100 in PBS) or

1× PBS with 0.1% Triton X-100, and incubated with the desired primary antibody. After several washes, disks were incubated with the desired secondary antibody (Alexa 350-, 488-, 594-, or 647-conjugated, Molecular Probes®, 1:100–1:1,000) and washed in PBS-T (0.1% Triton X-100 in PBS). The samples were mounted in Fluoro-Guard Antifade Reagent (Bio-Rad®) or Vectashield (Vector Laboratories®, H-1000). EdU (5-ethynyl-2'-deoxyuridine) assays were performed as previously described (Pallavi et al, 2012).

Caenorhabditis elegans

Caenorhabditis elegans worms were maintained under standard conditions (Stiernagle, 2006). To score embryonic lethality, mixed populations of N2 (N2 refers to the WT strain) and *lag-1(om13)* animals were synchronized at L1 larval stage (Porta-de-la-Riva et al, 2012). L1 animals were seeded on RNAi plates, that is, empty vector control or *lin-61(RNAi)* plates and let grown for 3 days at 25°C. Subsequently, for each study group, eight L4 animals (P0) were singled out, transferred onto new plates, and assessed for embryonic lethality, that is, 1 day after removing the P0 mothers from the plates, the proportion of embryos that had failed to hatch were determined for each group. Scoring of the protruding vulva (Pvl) phenotype was performed by culturing the animals for two generations. P0 animals were grown for 36 h at 25°C. Subsequently, for each study group, eight L4 animals (P0) were singled out and transferred onto new Nematode Growth Medium (NGM) worm culturing media plates where the proportion of animals in the progeny (F1) was assessed for the presence of protruding vulvas.

Data availability

The mass spectrometry proteomics data from this publication have been deposited to the ProteomeXchange Consortium via the PRIDE (Vizcaino et al, 2016) partner repository with the dataset identifier PXD004196. The ChIP-Seq data from this publication have been deposited in NCBI's Gene Expression Omnibus (Edgar et al, 2002) and are accessible through GEO Series accession number GSE100375: <https://www.ncbi.nlm.nih.gov/geo/query/acc.cgi?acc=GSE100375>.

Expanded View for this article is available online.

Acknowledgements

We thank Dr. S. Artavanis-Tsakonas, the members of the Artavanis-Tsakonas, Borggreffe, Kovall, and Rual laboratories, and the members of the University of Michigan Notch club. We thank Dr. M. Vidal and members of the CCSB (Harvard Medical School, Boston, USA) for sharing ORFeome and Y2H clones and the University of Michigan Vector Core Facility for the lentiviral shRNA plasmids. We are grateful to Drs. S. Li, Y. Sun, C. Kleer, I. Maillard, and X. Yu (University of Michigan, Ann Arbor, USA), Dr. J. Huang (Zhejiang University, China), J. Soelch and Dr. M. Kracht (University of Giessen, Germany), Dr. R. Liefke (Boston Children's Hospital, USA), Dr. W. Pear (University of Pennsylvania, USA), Dr. S. Bray (University of Cambridge, UK), and to I. Macinkovic and Dr. A. Brehm (University of Marburg, Germany) for providing us with reagents. We want to thank P. Käse and T. Schmidt-Wöll (University of Giessen, Germany) for excellent technical assistance as well as J. Rupp and Dr. S. Herold (University of Giessen, Germany) for the FACS sorting service. This work was supported by a Grant Award awarded to J.F.R. by the CONquer canCER Now (CONCERN)

Foundation; a Grant Award awarded to J.F.R. by the Association for Research of Childhood Cancer (AROCC); a Grant Award awarded to J.F.R. by the Childhood Brain Tumor Foundation (CBTF); an M-Cubed Grant awarded to J.F.R. and C.Y.L.; and funds from the University of Michigan Department of Pathology provided to J.F.R. This research was also supported, in part, by the National Institutes of Health (NIH) through University of Michigan Cancer Center Support Grant (P30 CA046592), NIGMS grant R01GM094231 awarded to A.I.N., NCI grant R01CA187903 awarded to J.F.R., and NCI grant 5R01CA178974-03 to R.A.K.

Author contributions

J-FR conceived and directed the project. TX and KHa designed and performed the Y2H experiments. S-SP, KPC, VB, KSJE-J, and AIN designed and performed the AP-MS analyses. DH and RAK designed and performed the ITC experiments. TX, S-SP, BDG, FF, HZ, EM, and TB designed and performed the other molecular, biochemical, and cell studies. KHo, LA, DMH, and C-YL designed and performed the *Drosophila* genetics experiments. MB performed the analysis of the *Drosophila* ChIP-seq data. TX, YS, and YD performed the ChIP-seq analyses. BG and YZ performed the HMM profile alignment analyses. IE and JC designed and performed the *C. elegans* genetics experiments. RK performed statistical analyses. J-FR wrote the manuscript, with contributions from other co-authors.

Conflict of interest

The authors declare that they have no conflict of interest.

References

- Almeida MS, Bray SJ (2005) Regulation of post-embryonic neuroblasts by *Drosophila* Grainyhead. *Mech Dev* 122: 1282–1293
- Amente S, Lania L, Majello B (2013) The histone LSD1 demethylase in stemness and cancer transcription programs. *Biochim Biophys Acta* 1829: 981–986
- Arai S, Miyazaki T (2005) Impaired maturation of myeloid progenitors in mice lacking novel Polycomb group protein MBT-1. *EMBO J* 24: 1863–1873
- Aster JC, Pear WS, Blacklow SC (2017) The varied roles of Notch in cancer. *Annu Rev Pathol* 12: 245–275
- Bocconi P, MacGrogan D, Scandura JM, Nimer SD (2003) The human L(3)MBT polycomb group protein is a transcriptional repressor and interacts physically and functionally with TEL (ETV6). *J Biol Chem* 278: 15412–15420
- Bonasio R, Lecona E, Reinberg D (2010) MBT domain proteins in development and disease. *Semin Cell Dev Biol* 21: 221–230
- Borggreffe T, Oswald F (2014) Keeping notch target genes off: a CSL corepressor caught in the act. *Structure* 22: 3–5
- Bray SJ (2006) Notch signalling: a simple pathway becomes complex. *Nat Rev Mol Cell Biol* 7: 678–689
- Collins KJ, Yuan Z, Kovall RA (2014) Structure and function of the CSL-KyoT2 corepressor complex: a negative regulator of Notch signaling. *Structure* 22: 70–81
- Di Stefano L, Walker JA, Burgio G, Corona DF, Mulligan P, Naar AM, Dyson NJ (2011) Functional antagonism between histone H3K4 demethylases *in vivo*. *Genes Dev* 25: 17–28
- Dreze M, Monachello D, Lurin C, Cusick ME, Hill DE, Vidal M, Braun P (2010) High-quality binary interactome mapping. *Methods Enzymol* 470: 281–315
- Edgar R, Domrachev M, Lash AE (2002) Gene Expression Omnibus: NCBI gene expression and hybridization array data repository. *Nucleic Acids Res* 30: 207–210

- Egger B, Gold KS, Brand AH (2010) Notch regulates the switch from symmetric to asymmetric neural stem cell division in the *Drosophila* optic lobe. *Development* 137: 2981–2987
- Friedmann DR, Wilson JJ, Kovall RA (2008) RAM-induced allostery facilitates assembly of a notch pathway active transcription complex. *J Biol Chem* 283: 14781–14791
- Fujimoto M, Takagi Y, Muraki K, Nozaki K, Yamamoto N, Tsuji M, Hashimoto N, Honjo T, Tanigaki K (2009) RBP-J promotes neuronal differentiation and inhibits oligodendroglial development in adult neurogenesis. *Dev Biol* 332: 339–350
- Go MJ, Eastman DS, Artavanis-Tsakonas S (1998) Cell proliferation control by Notch signaling in *Drosophila* development. *Development* 125: 2031–2040
- Goodfellow H, Krejci A, Moshkin Y, Verrijzer CP, Karch F, Bray SJ (2007) Gene-specific targeting of the histone chaperone asf1 to mediate silencing. *Dev Cell* 13: 593–600
- Greenwald I (2012) Notch and the awesome power of genetics. *Genetics* 191: 655–669
- Grimm C, Matos R, Ly-Hartig N, Steuerwald U, Lindner D, Rybin V, Muller J, Muller CW (2009) Molecular recognition of histone lysine methylation by the Polycomb group repressor dSfmbt. *EMBO J* 28: 1965–1977
- Gupta BP, Hanna-Rose W, Sternberg PW (2012) Morphogenesis of the vulva and the vulval-uterine connection. *WormBook* 1–20
- Guruharsha KG, Kankel MW, Artavanis-Tsakonas S (2012) The Notch signalling system: recent insights into the complexity of a conserved pathway. *Nat Rev Genet* 13: 654–666
- Harrison MM, Lu X, Horvitz HR (2007) LIN-61, one of two *Caenorhabditis elegans* malignant-brain-tumor-repeat-containing proteins, acts with the DRM and NuRD-like protein complexes in vulval development but not in certain other biological processes. *Genetics* 176: 255–271
- Hori K, Sen A, Artavanis-Tsakonas S (2013) Notch signaling at a glance. *J Cell Sci* 126: 2135–2140
- Janic A, Mendizabal L, Llamazares S, Rossell D, Gonzalez C (2010) Ectopic expression of germline genes drives malignant brain tumor growth in *Drosophila*. *Science* 330: 1824–1827
- Jarriault S, Greenwald I (2002) Suppressors of the egg-laying defective phenotype of sel-12 presenilin mutants implicate the CoREST corepressor complex in LIN-12/Notch signaling in *C. elegans*. *Genes Dev* 16: 2713–2728
- Johnson SE, Ilagan MX, Kopan R, Barrick D (2010) Thermodynamic analysis of the CSL × Notch interaction: distribution of binding energy of the Notch RAM region to the CSL beta-trefoil domain and the mode of competition with the viral transactivator EBNA2. *J Biol Chem* 285: 6681–6692
- Keller A, Nesvizhskii AI, Kolker E, Aebersold R (2002) Empirical statistical model to estimate the accuracy of peptide identifications made by MS/MS and database search. *Anal Chem* 74: 5383–5392
- Kopan R, Ilagan MX (2009) The canonical Notch signaling pathway: unfolding the activation mechanism. *Cell* 137: 216–233
- Kovall RA, Hendrickson WA (2004) Crystal structure of the nuclear effector of Notch signaling, CSL, bound to DNA. *EMBO J* 23: 3441–3451
- Kulic I, Robertson G, Chang L, Baker JH, Lockwood WW, Mok W, Fuller M, Fournier M, Wong N, Chou V, Robinson MD, Chun HJ, Gilks B, Kempkes B, Thomson TA, Hirst M, Minchinton AJ, Lam WL, Jones S, Marra M et al (2015) Loss of the Notch effector RBPJ promotes tumorigenesis. *J Exp Med* 212: 37–52
- Levitani D, Greenwald I (1995) Facilitation of lin-12-mediated signalling by sel-12, a *Caenorhabditis elegans* S182 Alzheimer's disease gene. *Nature* 377: 351–354
- Li L, Lyu X, Hou C, Takenaka N, Nguyen HQ, Ong CT, Cubenas-Potts C, Hu M, Lei EP, Bosco G, Qin ZS, Corces VG (2015a) Widespread rearrangement of 3D chromatin organization underlies polycomb-mediated stress-induced silencing. *Mol Cell* 58: 216–231
- Li X, Wang W, Wang J, Malovannaya A, Xi Y, Li W, Guerra R, Hawke DH, Qin J, Chen J (2015b) Proteomic analyses reveal distinct chromatin-associated and soluble transcription factor complexes. *Mol Syst Biol* 11: 775
- Liefke R, Oswald F, Alvarado C, Ferres-Marco D, Mittler G, Rodriguez P, Dominguez M, Borggreve T (2010) Histone demethylase KDM5A is an integral part of the core Notch-RBP-J repressor complex. *Genes Dev* 24: 590–601
- Ling PD, Hayward SD (1995) Contribution of conserved amino acids in mediating the interaction between EBNA2 and CBF1/RBPJk. *J Virol* 69: 1944–1950
- Louvi A, Artavanis-Tsakonas S (2012) Notch and disease: a growing field. *Semin Cell Dev Biol* 23: 473–480
- Meier K, Mathieu EL, Finkernagel F, Reuter LM, Scharfe M, Doehlemann G, Jarek M, Brehm A (2012) LINT, a novel dL(3)mbt-containing complex, represses malignant brain tumour signature genes. *PLoS Genet* 8: e1002676
- Mellacheruvu D, Wright Z, Couzens AL, Lambert JP, St-Denis NA, Li T, Miteva YV, Hauri S, Sardi ME, Low TY, Halim VA, Bagshaw RD, Hubner NC, Al-Hakim A, Bouchard A, Faubert D, Fermin D, Dunham WH, Goudreaux M, Lin ZY et al (2013) The CRAPome: a contaminant repository for affinity purification-mass spectrometry data. *Nat Methods* 10: 730–736
- Metzger E, Wissmann M, Yin N, Muller JM, Schneider R, Peters AH, Gunther T, Buettner R, Schule R (2005) LSD1 demethylates repressive histone marks to promote androgen-receptor-dependent transcription. *Nature* 437: 436–439
- Min J, Allali-Hassani A, Nady N, Qi C, Ouyang H, Liu Y, MacKenzie F, Vedadi M, Arrowsmith CH (2007) L3MBTL1 recognition of mono- and dimethylated histones. *Nat Struct Mol Biol* 14: 1229–1230
- Morgan TH (1917) The theory of the gene. *Am Nat* 51: 513–544
- Moshkin YM, Kan TW, Goodfellow H, Bezstarosti K, Maeda RK, Pilyugin M, Karch F, Bray SJ, Demmers JA, Verrijzer CP (2009) Histone chaperones ASF1 and NAP1 differentially modulate removal of active histone marks by LID-RPD3 complexes during NOTCH silencing. *Mol Cell* 35: 782–793
- Mulligan P, Yang F, Di Stefano L, Ji JY, Ouyang J, Nishikawa JL, Toiber D, Kulkarni M, Wang Q, Najafi-Shoushtari SH, Mostoslavsky R, Gygi SP, Gill G, Dyson NJ, Naar AM (2011) A SIRT1-LSD1 corepressor complex regulates Notch target gene expression and development. *Mol Cell* 42: 689–699
- Nady N, Krichevsky L, Zhong N, Duan S, Tempel W, Amaya MF, Ravichandran M, Arrowsmith CH (2012) Histone recognition by human malignant brain tumor domains. *J Mol Biol* 423: 702–718
- Nesvizhskii AI, Keller A, Kolker E, Aebersold R (2003) A statistical model for identifying proteins by tandem mass spectrometry. *Anal Chem* 75: 4646–4658
- Noma K, Allis CD, Grewal SI (2001) Transitions in distinct histone H3 methylation patterns at the heterochromatin domain boundaries. *Science* 293: 1150–1155
- Oswald F, Kostezka U, Astrahantseff K, Bourteele S, Dillinger K, Zechner U, Ludwig L, Wilda M, Hameister H, Knochel W, Liptay S, Schmid RM (2002) SHARP is a novel component of the Notch/RBP-Jkappa signalling pathway. *EMBO J* 21: 5417–5426
- Pallavi SK, Ho DM, Hicks C, Miele L, Artavanis-Tsakonas S (2012) Notch and Mef2 synergize to promote proliferation and metastasis through JNK signal activation in *Drosophila*. *EMBO J* 31: 2895–2907
- Pedrioli PG (2010) Trans-proteomic pipeline: a pipeline for proteomic analysis. *Methods Mol Biol* 604: 213–238

- Porta-de-la-Riva M, Fontrodona L, Villanueva A, Ceron J (2012) Basic *Caenorhabditis elegans* methods: synchronization and observation. *J Vis Exp* e4019
- Priess JR (2005) Notch signaling in the *C. elegans* embryo. *WormBook* 1–16
- Qiao L, Lissemore JL, Shu P, Smardon A, Gelber MB, Maine EM (1995) Enhancers of *glp-1*, a gene required for cell-signaling in *Caenorhabditis elegans*, define a set of genes required for germline development. *Genetics* 141: 551–569
- Reddy BV, Rauskolb C, Irvine KD (2010) Influence of fat-hippo and notch signaling on the proliferation and differentiation of *Drosophila* optic neuroepithelia. *Development* 137: 2397–2408
- Richter C, Oktaba K, Steinmann J, Muller J, Knoblich JA (2011) The tumour suppressor L(3)mbt inhibits neuroepithelial proliferation and acts on insulator elements. *Nat Cell Biol* 13: 1029–1039
- Rual JF, Ceron J, Koreth J, Hao T, Nicot AS, Hirozane-Kishikawa T, Vandenhaute J, Orkin SH, Hill DE, van den Heuvel S, Vidal M (2004) Toward improving *Caenorhabditis elegans* phenome mapping with an ORFeome-based RNAi library. *Genome Res* 14: 2162–2168
- Saj A, Arziman Z, Stempfle D, van Belle W, Sauder U, Horn T, Durrenberger M, Paro R, Boutros M, Merdes G (2010) A combined *ex vivo* and *in vivo* RNAi screen for notch regulators in *Drosophila* reveals an extensive notch interaction network. *Dev Cell* 18: 862–876
- Shevchenko A, Tomas H, Havlis J, Olsen JV, Mann M (2006) In-gel digestion for mass spectrometric characterization of proteins and proteomes. *Nat Protoc* 1: 2856–2860
- Shi Y, Lan F, Matson C, Mulligan P, Whetstine JR, Cole PA, Casero RA, Shi Y (2004) Histone demethylation mediated by the nuclear amine oxidase homolog LSD1. *Cell* 119: 941–953
- Soding J (2005) Protein homology detection by HMM-HMM comparison. *Bioinformatics* 21: 951–960
- Stiernagle T (2006) Maintenance of *C. elegans*. *WormBook* 1–11
- Tang M, Shen H, Jin Y, Lin T, Cai Q, Pinard MA, Biswas S, Tran Q, Li G, Shenoy AK, Tongdee E, Lin S, Gu Y, Law BK, Zhou L, McKenna R, Wu L, Lu J (2013) The malignant brain tumor (MBT) domain protein SFMBT1 is an integral histone reader subunit of the LSD1 demethylase complex for chromatin association and epithelial-to-mesenchymal transition. *J Biol Chem* 288: 27680–27691
- Tanigaki K, Honjo T (2010) Two opposing roles of RBP-J in Notch signaling. *Curr Top Dev Biol* 92: 231–252
- Taniguchi Y, Furukawa T, Tun T, Han H, Honjo T (1998) LIM protein KyoT2 negatively regulates transcription by association with the RBP-J DNA-binding protein. *Mol Cell Biol* 18: 644–654
- Trojer P, Li G, Sims RJ III, Vaquero A, Kalakonda N, Bocconi P, Lee D, Erdjument-Bromage H, Tempst P, Nimer SD, Wang YH, Reinberg D (2007) L3MBTL1, a histone-methylation-dependent chromatin lock. *Cell* 129: 915–928
- VanderWielen BD, Yuan Z, Friedmann DR, Kovall RA (2011) Transcriptional repression in the Notch pathway: thermodynamic characterization of CSL-MINT (Msx2-interacting nuclear target protein) complexes. *J Biol Chem* 286: 14892–14902
- Vasyutina E, Lenhard DC, Wende H, Erdmann B, Epstein JA, Birchmeier C (2007) RBP-J (Rbbsuh) is essential to maintain muscle progenitor cells and to generate satellite cells. *Proc Natl Acad Sci USA* 104: 4443–4448
- Vizcaino JA, Csordas A, del-Toro N, Dianes JA, Griss J, Lavidas I, Mayer G, Perez-Riverol Y, Reisinger F, Ternent T, Xu QW, Wang R, Hermjakob H (2016) 2016 update of the PRIDE database and its related tools. *Nucleic Acids Res* 44: D447–D456
- Wang J, Scully K, Zhu X, Cai L, Zhang J, Prefontaine GG, Kronen A, Ohgi KA, Zhu P, Garcia-Bassets I, Liu F, Taylor H, Lozach J, Jayes FL, Korach KS, Glass CK, Fu XD, Rosenfeld MG (2007) Opposing LSD1 complexes function in developmental gene activation and repression programmes. *Nature* 446: 882–887
- Wang H, Zang C, Liu XS, Aster JC (2015) The role of Notch receptors in transcriptional regulation. *J Cell Physiol* 230: 982–988
- West LE, Roy S, Lachmi-Weiner K, Hayashi R, Shi X, Appella E, Kutateladze TG, Gozani O (2010) The MBT repeats of L3MBTL1 link SET8-mediated p53 methylation at lysine 382 to target gene repression. *J Biol Chem* 285: 37725–37732
- Wisnar J, Loffler T, Habtemichael N, Vef O, Geissen M, Zirwes R, Altmeyer W, Sass H, Gateff E (1995) The *Drosophila melanogaster* tumor suppressor gene lethal(3)malignant brain tumor encodes a proline-rich protein with a novel zinc finger. *Mech Dev* 53: 141–154
- Yasugi T, Sugie A, Umetsu D, Tabata T (2010) Coordinated sequential action of EGFR and Notch signaling pathways regulates proneural wave progression in the *Drosophila* optic lobe. *Development* 137: 3193–3203
- Yatim A, Benne C, Sobhian B, Laurent-Chabalier S, Deas O, Judde JG, Lelievre JD, Levy Y, Benkirane M (2012) NOTCH1 nuclear interactome reveals key regulators of its transcriptional activity and oncogenic function. *Mol Cell* 48: 445–458
- Yohn CB, Pusateri L, Barbosa V, Lehmann R (2003) l(3)malignant brain tumor and three novel genes are required for *Drosophila* germ-cell formation. *Genetics* 165: 1889–1900
- Yuan Z, Friedmann DR, VanderWielen BD, Collins KJ, Kovall RA (2012) Characterization of CSL (CBF-1, Su(H), Lag-1) mutants reveals differences in signaling mediated by Notch1 and Notch2. *J Biol Chem* 287: 34904–34916
- Zacharioudaki E, Housden BE, Garinis G, Stojnic R, Delidakis C, Bray SJ (2016) Genes implicated in stem cell identity and temporal programme are directly targeted by Notch in neuroblast tumours. *Development* 143: 219–231
- Zhang Z, Zhou L, Yang X, Wang Y, Zhang P, Hou L, Hu X, Xing Y, Liu Y, Li W, Han H (2012) Notch-RBP-J-independent marginal zone B cell development in IgH transgenic mice with VH derived from a natural polyreactive antibody. *PLoS One* 7: e38894



License: This is an open access article under the terms of the Creative Commons Attribution-NonCommercial-NoDerivs 4.0 License, which permits use and distribution in any medium, provided the original work is properly cited, the use is non-commercial and no modifications or adaptations are made.